

# LayerAct: Advanced Activation Mechanism for Robust Inference of CNNs

Kihyuk Yoon, Chiehyeon Lim

UNIST, Ulsan, Republic of Korea  
kh.yoon@unist.ac.kr, chlim@unist.ac.kr

## Abstract

In this work, we propose a novel activation mechanism called LayerAct for CNNs. This approach is motivated by our theoretical and experimental analyses, which demonstrate that Layer Normalization (LN) can mitigate a limitation of existing activation functions regarding noise robustness. However, LN is known to be disadvantageous in CNNs due to its tendency to make activation outputs homogeneous. The proposed method is designed to be more robust than existing activation functions by reducing the upper bound of influence caused by input shifts without inheriting LN's limitation. We provide analyses and experiments showing that LayerAct functions exhibit superior robustness compared to ElementAct functions. Experimental results on three clean and noisy benchmark datasets for image classification tasks indicate that LayerAct functions outperform other activation functions in handling noisy datasets while achieving superior performance on clean datasets in most cases.

## Code & Appendix —

<https://github.com/KihyukYoon/LayerAct>

## Introduction

Most existing activation functions follow *element-level activation* (*ElementAct*) mechanisms, meaning the functions apply independently to each element of the input. However, we identified a limitation in the method: their robustness varies across samples. This is because their robustness relies on the saturation state, where the activation output for a specific range converges to a certain value. For example, in a layer with ReLU (Nair and Hinton 2010), the elements of the output remain unaffected by input shifts only when they are in the saturation state, specifically when the input and shifted input of the elements are smaller than zero. Consequently, existing activation functions can ensure robustness only when a sufficient number of elements are in the saturation state, not when there are fewer elements in that state.

We found that Layer Normalization (LN; Ba, Kiros, and Hinton (2016)) can address this limitation of ElementAct functions. Our theoretical and experimental analyses reveal that placing LN right before the activation (i.e., using the output of LN as the input to the activation) can enhance the

robustness of networks. However, previous studies have reported that Convolutional Neural Networks (CNNs) with LN tend to perform poorly on clean datasets, mainly due to LN's tendency to lead to homogeneous activation. These claims are supported by our empirical results on the representation of the last layer in CNNs with LN. Therefore, our goal is to develop a method that captures the noise-robustness benefits of LN without inheriting its homogeneity limitations.

To achieve this goal, we propose a novel activation method, the Layer-level Activation (LayerAct) mechanism. Unlike the ElementAct mechanism, our proposed method utilizes layer-direction normalization for activation, but the activation output is far different from that of ElementAct with LN. This enables LayerAct to absorb LN's robustness benefit for activation while avoiding its homogeneity limitation. Additionally, LayerAct functions are not subject to the trade-off issue between two important properties of activation, one-side saturation and zero-like activation mean (Clevert, Unterthiner, and Hochreiter 2016; Qiu, Xu, and Cai 2018), which are faced by ElementAct functions (for details, see Appendix A). These two benefits of LayerAct functions, enhanced robustness and freedom from the trade-off problem, underscore their potential to outperform existing ElementAct functions on both noisy and clean datasets.

Experimental analysis with the MNIST dataset demonstrates that LayerAct functions have the following properties: (1) the mean activation of LayerAct functions is zero-like, and (2) the output fluctuation due to noisy input is smaller with these functions than with ElementAct functions. We compared the performance of the residual networks (ResNets; He et al. (2016)) with LayerAct functions to those with other ElementAct functions on three image classification tasks.

Our contributions can be summarized as follows:

- We identify a previously unrecognized limitation in existing activation mechanisms, namely a large variance of noise-robustness across samples.
- We present analysis and experimental evidence showing that while LN can address this limitation, it also causes the final layer representation in CNNs to be less distinguishable between samples with different labels.
- We introduce LayerAct that exhibit greater robustness than existing ElementAct functions, without the homo-

geneity limitation of LN.

- We empirically evaluate LayerAct functions, and they show superior performance on both clean and noisy datasets in most cases.

## Backgrounds

In this section, we provide the background for the analyses presented in the remainder of this paper, including the definition of *activation scale* and a review of normalizations.

### Activation Scale

In some activation functions, a function bounded between one and zero characterizes their non-linearity. We define this function, denoted as  $s$ , and its output as the *activation scale function* and *activation scale*, respectively.

Consider a layer in a multi-layer perceptron with linear projection and an activation function. Given a  $r$ -dimensional vector  $x = (x_1, \dots, x_r)^T$ , a weight matrix  $W \in \mathbb{R}^{r \times D}$ , where  $d$  is the dimension of activation input (e.g.,  $D = C \times H \times W$  for image), and a non-linear activation function  $f$ , the activation output is  $a = f(y)$ , where  $y = W^T x$ . With an activation scale function  $s$ , the activation output and gradient of forward and backward passes are:

$$a_i = y_i s(y_i), \quad \frac{\partial a_i}{\partial y_i} = s(y_i) + y_i \frac{\partial s(y_i)}{\partial y_i}, \quad (1)$$

where  $s$  is increasing and  $s(y_i) > 0$  if  $y_i > 0$ . For example, the activation scale function for the  $i^{\text{th}}$  element in the SiLU (Elfving, Uchibe, and Doya 2018) is presented as follows:

$$s^{\text{SiLU}}(y_i) = \text{sigmoid}(y_i) = \frac{1}{1 + e^{-y_i}}, \quad (2)$$

where *sigmoid* and  $s^{\text{SiLU}}$  represent the Logistic Sigmoid function, and the activation scale functions of SiLU, respectively. For further discussion, we define a specific activation scale function  $s$ .

**Definition 1 (Activation Scale Function)** *The activation scale function  $s$  is an increasing Lipschitz continuous function that is bounded between zero and one:*

$$s(0) = 1/2, \quad |s(a) - s(b)| \leq K |a - b| \quad \forall a, b \in \mathbb{R}. \quad (3)$$

For example, the activation scale of SiLU satisfies this, as the activation scale is *sigmoid*( $y_i$ ). Meanwhile, the activation scale also determines the saturation state of the activation functions, which occurs when  $s(y_i) \simeq 0$ .

In conclusion, the activation scale function plays a crucial role in providing non-linearity during the forward pass, controlling the gradient during the backward pass, and determining the saturation state of the activation function.

### Revisiting Normalizations in CNNs

Normalization layers re-scale and re-center both the input and the gradient during forward and backward propagation, respectively. The normalization output  $n_i$  from the normalization input  $y_i$  is:

$$n_i = \gamma_i \cdot \frac{y_i - \mu_y}{\sigma_y} + \beta_i, \quad (4)$$

where  $\gamma_i$  and  $\beta_i$  are the learnable parameters of the affine function,  $D$  is the normalizing dimension, and  $\mu_y$  and  $\sigma_y$  are:

$$\mu_y = \frac{1}{D} \sum_{i=1}^D y_i, \quad \sigma_y = \sqrt{\frac{1}{D} \sum_{i=1}^D (y_i - \mu_y)^2}, \quad (5)$$

the mean and variance of the input  $y$ , respectively. Normalization layers can stabilize the network training by re-scaling and re-centering as shown in Equation 4. The dimension  $D$  varies according to the normalization methods,  $D = N \times H \times W$  for Batch Normalization (BN; Ioffe and Szegedy (2015)) and  $D = C \times H \times W$  for LN, where  $N$ ,  $C$ ,  $H$ , and  $W$  denote the size of the batch size, channel, height, and width of the image dataset.

BN has achieved great success in computer vision tasks within CNN-based networks and remains dominant in the field. In contrast, LN is less preferred compared to BN, largely due to the inferior performance of networks using LN. Previous studies have attributed this underperformance to LN’s tendency to produce homogeneous outputs (Lubana, Dick, and Tanaka 2021; Labatie et al. 2021).

## Problems Analysis and Research Motivation

In this section, we present our motivation, specifically, we focus on: (1) an analysis of the limitations of existing activation functions, and (2) theoretical and empirical analyses of the advantages and disadvantages of LN in CNNs.

### Large Variance of Activation Robustness

To analyze the robustness, we define *activation fluctuation* that can represent the influence of the shift of inputs.

**Definition 2 (Activation Fluctuation)** *Let  $\epsilon = (\epsilon_1, \epsilon_2, \dots, \epsilon_D)^T$  be the input shift vector, which is independent of the input vector  $y$ . We define activation fluctuation as  $\|f(y + \epsilon) - f(y)\| \leq c$ , where the constant  $c$  is the upper bound of activation fluctuation.*

The lower the upper bound  $c$  is, the lower the variance of robustness across samples. We can define the activation fluctuation of ElementAct functions.

**Definition 3 (Activation Fluctuation of Element-level Activation Functions)** *Let  $\hat{y}_i = y_i + \epsilon_i$  be the input with a shift. The activation fluctuation of an ElementAct function  $f$  is given by:*

$$\begin{aligned} \|f(\hat{y}) - f(y)\| &= \sum_{i=1}^D |\hat{y}_i s(\hat{y}_i) - y_i s(y_i)| \\ &= \sum_{i=1}^D |y_i (s(\hat{y}_i) - s(y_i)) + \epsilon_i s(\hat{y}_i)|. \end{aligned} \quad (6)$$

A sample will exhibit a small  $\|f(\hat{y}) - f(y)\|$  if a sufficient number of its elements are in a saturation state. However, ElementAct functions do not ensure that all samples have a sufficient number of elements in the saturation

Data	BN	None	LN	BN, LN	LN, BN
C10	91.29	88.51	88.24	90.65	89.73
C10-C	69.92	67.43	74.5	74.34	72.55
C10	91.45	88.29	87.53	89.74	90.17
C10-C	70.12	68.94	74.96	73.69	72.47

Table 1: Classification performance of original ResNet20 and three variants of ResNet20 with ReLU (upper) and SiLU (lower) on CIFAR10 (C10) and CIFAR10-C (C10-C).

state. More specifically, the activation fluctuation is upper-bounded when not all elements are in the saturation state, where  $y_i > 0$  for all  $i$ :

$$\|f(\hat{y}) - f(y)\| \leq \sum_{i=1}^D (y_i |s(\hat{y}_i) - s(y_i)| + |\epsilon_i| \cdot s(\hat{y}_i)). \quad (7)$$

Considering Definition 1, the upper bound of  $\|s(\hat{y}) - s(y)\|$  and  $\|s(\hat{y})\|$  of ElementAct functions are given by the following, respectively:

$$\|s(\hat{y}) - s(y)\| \leq \sum_{i=1}^D K |\epsilon_i|, \quad \|s(\hat{y}_i)\| \leq d. \quad (8)$$

Equation 7 demonstrates that activation scale is closely related to the activation fluctuation. Samples with large  $\|s(\hat{y}) - s(y)\|$  and  $\|s(\hat{y})\|$  are not robust to the input shift  $\epsilon$ . Thus, a method that has a lower upper bound for  $\|s(\hat{*}) - s(*)\|$  and  $\|s(\hat{*})\|$  will reduce the upper bound of activation fluctuation, resulting in a low variance of robustness across samples.

### Empirical Analysis on Normalizations in CNNs

To empirically analyze the impact of BN and LN in CNNs, we conducted a series of experiments using the CIFAR10 (Krizhevsky 2009) dataset with the ResNet20 architecture. In the original ResNet20, BN layers are positioned immediately before the activation layers. For our experiments, we designed four variants of ResNet20: (1) eliminating BN layers entirely (ResNet20-None), (2) replacing BN layers with LN layers (ResNet20-LN), (3) adding LN layers before the BN layers (ResNet20-(LN, BN)), and (4) adding LN layers after the BN layers (ResNet20-(BN, LN)).

Table 1 demonstrates the performance of the ResNet20 variants with different normalization on both CIFAR10 and CIFAR10-C (Hendrycks and Dietterich 2019). The networks were trained on CIFAR10. The CIFAR10-C dataset serves as a noise-robustness benchmark, incorporating 19 out-of-distribution (OOD) corruptions of CIFAR10. This dataset includes a total of 19 distinct corruptions, each with five levels of severity, organized into five categories: noise, blur, digital, weather, and extra. We evaluated the models using two activation functions: ReLU and SiLU. The table reports the average mean accuracy over 30 runs, with "Norm" and "Act" denoting the normalization and activation, respectively. The experimental results show that the use of LN

alone leads to inferior performance on the clean dataset, CIFAR10. Specifically, networks with LN alone showed inferior results compared to those without normalization, which aligns with findings from previous studies.

LN and other batch-free normalizations have been shown to block the negative effect of BN on robustness of networks (?). Interestingly, our experiments reveal a detailed robustness advantage of LN, which can lead to robust activation, and this has not been emphasized in previous studies. On the noisy dataset, CIFAR10-C, the networks incorporating LN demonstrated better performance than those without LN. Notably, when LN is applied immediately before the activation layers, as in ResNet20-LN and ResNet20-(BN, LN), these networks outperformed their counterparts, ResNet20-None and ResNet20-(LN, BN), on noisy datasets, despite underperforming on the clean dataset. This suggests that LN may provide a robustness benefit, which is closely related to activation.

### LN and Activation Robustness

Based on the experimental result from the experimental analysis, we analyzed the relationship between LN and activation robustness. Here, we only consider LN without an affine function. In this case, the normalized output  $n_i$ , the normalized output with a shift  $\hat{n}_i$ , the activation output  $a$ , and activation output with shift  $\hat{a}$  are as follows:

$$n_i = \frac{y_i - \mu_y}{\sqrt{\sigma_y^2 + \alpha}}, \quad \hat{n}_i = \frac{\hat{y}_i - \hat{\mu}_y}{\sqrt{\hat{\sigma}_y^2 + \alpha}} \quad (9)$$

$$a_i = n_i s(n_i), \quad \hat{a}_i = \hat{n}_i s(\hat{n}_i),$$

where  $\hat{\mu}_y$  and  $\hat{\sigma}_y^2$  are the layer-direction mean and variance of  $\hat{y}$ . The activation fluctuation using Equations 4 and 9 are:

**Definition 4 (Activation Fluctuation of ElementAct Functions with LN)** Let  $\epsilon_i$ ,  $\hat{y}_i$ , and  $\hat{n}_i$  of the  $i^{\text{th}}$  normalization layer be the shift of the input, the input with the shift, and the output from the input. The activation fluctuation of an ElementAct function  $f$  is:

$$\|f(\hat{n}) - f(n)\| = \sum_{i=1}^D |\hat{n}_i s(\hat{n}_i) - n_i s(n_i)|$$

$$\lesssim \sum_{i=1}^D (|n_i| \cdot |s(\hat{n}_i) - s(n_i)|) \quad (10)$$

$$+ \sum_{i=1}^D \left( \frac{|\epsilon - \mu_\epsilon| \cdot s(\hat{n}_i)}{\sqrt{\sigma_y^2 + \alpha}} \right),$$

where  $\sqrt{\sigma_y^2 + \alpha + \sigma_\epsilon^2} \approx \sqrt{\sigma_y^2 + \alpha}$  and  $\sigma_y \gg \sigma_\epsilon$ .

For the detailed derivation process of the equations, see Appendix B. In the previous section, we discussed that reducing the magnitudes of the terms of the activation scale effectively decreases the upper bound of activation fluctuation, thereby reducing the variance of activation robustness across samples. Considering Definitions 1 and 4, the upper



Figure 1: Plots of the last layer representation in ResNet20 with BN (left), and LN (right).

bound of  $\|s(\hat{n}) - s(n)\|$  and  $\|s(\hat{n})\|$  is given as follows:

$$\|s(\hat{n}) - s(n)\| < \sum_{i=1}^D \frac{K |\epsilon_i - \mu_\epsilon|}{\sqrt{\sigma_y^2 + \alpha}}, \quad \|s(\hat{n}_i)\| \ll d, \quad (11)$$

which are lower than those of ElementAct functions without normalization (see Equation 8), specifically considering that  $\frac{|\epsilon_i - \mu_\epsilon|}{\sqrt{\sigma_y^2 + \alpha}} < 1$ , where  $\sigma_y \gg \sigma_\epsilon$ . This reveals that LN can improve activation robustness not only by re-scaling and re-centering, but also by affecting the activation scale. The experimental results in Table 1 support our analysis, demonstrating that networks with LN are much more robust compared to those without normalization.

### Homogeneity Limitation of LN across Labels

It is well-known that LN produces homogeneous outputs across samples by normalizing the mean and variance of the input. However, this homogeneity extends beyond its output: LN causes activations to become similar across samples. Specifically, when LN is placed right before the activation function, producing outputs  $ns(n)$ , it loses the mean and variance statistics of input  $y$ . Here, we provide experimental results showing that LN produces homogeneous representations across samples, even those with different labels.

Figure 1 illustrates the last layer representation in ResNet20 with BN and LN on CIFAR10, visualized using Isomap embedding (Tenenbaum, de Silva, and Langford 2000). The figure demonstrates that the representation of the network with LN is less distinguishable between data points with different labels compared to the network with BN, which provides evidence of how LN leads to inferior performance on clean datasets. This reduced distinguishability is due to the similar output statistics of LN across samples. The variances of the output mean and variance in networks with LN are 0.0001 and 0.00072, respectively, which are substantially lower than those observed with BN (0.00073 and 0.00803, respectively). These experimental results align with previous studies, suggesting that LN’s tendency to produce homogeneous outputs is a key limitation.

### Summary

In this section, we presented analyses and empirical results highlighting that existing activation functions have a limitation regarding noise robustness, which LN can address. However, LN is not a preferred normalization method for

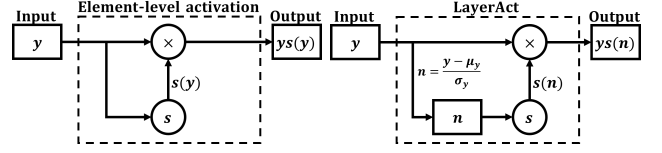


Figure 2: The mechanisms of the ElementAct (left) and proposed layer-level activation (right).

CNNs due to its homogeneity limitation. Motivated by this, our goal is to develop a method that captures the robustness benefit of LN without inheriting its limitation.

## Layer-level Activation

In this section, we introduce LayerAct mechanism, a novel approach that operates differently from existing ElementAct functions, as illustrated in Figure 2.

### LayerAct Mechanism

A function that follows LayerAct mechanism is defined as the product of the input  $y_i$  and the activation scale  $s(n_i)$ , which uses the layer-normalized input  $n_i$ . The forward and backward pass of a LayerAct function are given by:

$$a_i = y_i s(n_i), \quad n_i = \frac{(y_i - \mu_y)}{\sqrt{\sigma_y^2 + \alpha}}, \quad (12)$$

$$\begin{aligned} \frac{\partial \mathcal{L}}{\partial \mu_y} &= \sum_{i=1}^D \frac{\partial \mathcal{L}}{\partial a_i} \cdot \frac{\partial s(n_i)}{\partial n_i} \cdot \frac{-y_i}{\sqrt{\sigma_y^2 + \alpha}}, \\ \frac{\partial \mathcal{L}}{\partial \sigma_y^2} &= \sum_{i=1}^D \frac{\partial \mathcal{L}}{\partial a_i} \cdot \frac{\partial s(n_i)}{\partial n_i} \cdot \frac{-y_i \cdot n_i}{2(\sigma_y^2 + \alpha)}, \\ \frac{\partial \mathcal{L}}{\partial y_i} &= \frac{\partial \mathcal{L}}{\partial a_i} s(n_i) + \frac{\partial \mathcal{L}}{\partial a_i} \cdot \frac{\partial s(n_i)}{\partial n_i} \cdot \frac{y_i}{\sqrt{\sigma_y^2 + \alpha}} \\ &\quad + \frac{1}{D} \cdot \frac{\partial \mathcal{L}}{\partial \mu_y} + \frac{2(y_i - \mu_y)}{D} \cdot \frac{\partial \mathcal{L}}{\partial \sigma_y^2}, \end{aligned} \quad (13)$$

respectively, where  $\alpha > 0$  is a constant for stability, and  $\mu_y$  and  $\sigma_y^2$  are layer-direction mean and variance, respectively.

For the stability of learning and inference, ensuring the continuity of activation outputs across the entire space is essential. While traditional ElementAct functions, such as ReLU, LReLU (Maas et al. 2013), and PReLU (He et al. 2015), do not require a continuous activation scale at zero (given that the activation output  $y_i s(y_i)$  remains continuous at zero), LayerAct functions need special consideration, as the activation output  $y_i s(n_i)$  is discontinuous if the activation scale function is not continuous.

Given such requirements for the activation scale functions, functions that satisfy Definition 1 are suitable for use as LayerAct functions. In this work, we propose two basic LayerAct functions, LA-SiLU and LA-HardSiLU, which utilize the Sigmoid and HardSigmoid functions as activation

scale functions, respectively. The activation outputs of these functions are as follows:

$$\begin{aligned} a^{LA-SiLU} &= \frac{y_i}{1 + e^{-n_i}}, \\ a^{LA-HardSiLU} &= \min\left(y_i, \max\left(\frac{y_i \cdot n_i}{6} + \frac{y_i}{2}, 0\right)\right). \end{aligned} \quad (14)$$

For the HardSigmoid of LA-HardSiLU, we used the function of Howard et al. (2019), which is a good approximation of Sigmoid.

## Benefits and Properties of LayerAct

**Diverse Activation Output** We discussed that LN tends to produce homogeneous activation outputs, as the mean and variance of  $n_i$  are similar across all samples. In contrast, LayerAct functions are designed to preserve these diverse representations by transferring the statistics of the activation input  $y$  to the activation output  $a$ . This difference is from the different activation outputs of activation with LN and LayerAct,  $n_i s(n_i)$  and  $y_i s(n_i)$ , respectively. Due its unique output, LayerAct can maintain the input statistics within the activation outputs, resulting in much more diverse representations. For details, see Appendices C and D.

**Noise-robustness of LayerAct** From here, we begin by establishing that the activation fluctuation of LayerAct is also related to the two terms of the activation scale function,  $\|s(\hat{*}) - s(*)\|$  and  $\|s(\hat{*})\|$ , as outlined in previous sections. Subsequently, we show that these two terms for LayerAct are bound to be lower than those of ElementAct. We can define the activation fluctuation of LayerAct as follows.

**Definition 5 (Activation Fluctuation of LayerAct Functions)** *The activation fluctuation of a LayerAct activation function  $g$ , where  $\hat{n}_i = (\hat{y}_i - \mu_{\hat{y}}) / \sigma_{\hat{y}}$  denotes the  $i^{\text{th}}$  noisy normalized input, is defined as:*

$$\begin{aligned} \|g(\hat{y}) - g(y)\| &= \sum_{i=1}^D |\hat{y}_i s(\hat{n}_i) - y_i s(n_i)| \\ &= \sum_{i=1}^D |y_i (s(\hat{n}_i) - s(n_i)) + \epsilon_i s(\hat{n}_i)|. \end{aligned} \quad (15)$$

This definition enables us to establish an upper bound for the activation fluctuation of LayerAct functions as follows:

$$\|g(\hat{y}) - g(y)\| \leq \sum_{i=1}^D (|y_i| |s(\hat{n}_i) - s(n_i)| + |\epsilon_i| |s(\hat{n}_i)|). \quad (16)$$

The terms of LayerAct’s activation scale functions,  $\|s(\hat{n}) - s(n)\|$  and  $\|s(\hat{n})\|$ , align precisely with those of the activation with LN, as indicated in Equation 11. Comparing Equations 8 and 11 reveals that LayerAct functions have a lower upper bound of activation fluctuation, similar to activation with LN. This reduction is achieved without the direct re-centering and re-scaling of the activation output. Therefore, it suggests that networks with LayerAct are likely to exhibit improved robustness during the forward pass.

**Addressing the Trade-off** LayerAct can address another limitation of existing activation functions, namely a trade-off between two important properties of activation: one-side saturation and zero-like activation mean. The key distinction in saturation between the element-level and LayerAct functions is that element-level functions have a fixed saturation state at a certain point of activation output, whereas the saturation state of LayerAct functions depends on layer-dimension normalized inputs. Consequently, LayerAct functions can still reach a saturation state where  $s(n_i) \simeq 0$ , yet without constraining the activation output space, enabling larger negative outputs (e.g., consider a layer where  $\mu_y \ll 0$ ). For details of the trade-off, see Appendix E.

## Relationship between Normalization

LayerAct functions have unique benefits that ElementAct functions cannot achieve. Therefore, it is important to select normalization methods that preserve the diversity of statistics across samples to maximize the advantages of LayerAct functions. With this consideration, batch-direction normalizations such as BN or Decorrelated Batch Normalization (DBN; Huang et al. (2018)) are identified as the most effective choices for CNNs with LayerAct functions. Conversely, other normalization methods like LN or Switch Normalization (SwitchNorm; Luo et al. (2019)) are less favored. For the details and experiments, see Appendices G, H, and I.

## Experiments

In this section, we present the experimental analysis and results of LayerAct. For the detailed experimental setting to ensure reproducibility, see Appendix F.

### Experimental Analysis on MNIST

In this subsection, we empirically analyze the properties of LayerAct discussed in the previous section: (1) diverse last layer representation between samples of different labels (2) activation robustness, and (3) zero-like activation mean. We trained a network with a single layer that containing 512 elements on the MNIST training dataset without any noise to observe the behavior of LayerAct functions during training.

**Ensuring Diverse Representation** One of the key properties of LayerAct is that it does not produce homogeneous outputs, unlike LN, ensuring diverse representations in networks. Figure 3 shows the final layer representation of ResNet20 with LA-SiLU without normalization or BN. LayerAct has more diverse representations than ResNet20 with LN and ReLU (Figure 1), despite utilizing layer-direction normalization. This is due to the activation output, which is the product of the activation input  $y$  and the activation scale  $s(n)$  (see Equation 12). This mechanism allows networks with BN and LayerAct to achieve better performance on clean datasets compared to those using LN.

**Activation Robustness** To confirm the robustness of LayerAct functions, we computed the activation fluctuation as defined in Definitions 3 and 5 using the network trained on the clean MNIST dataset. For the noisy input  $\hat{y}_i$ , we used two different noises with a normal distribution: one with a



Figure 3: Plots of the last layer representation in ResNet20 with LA-SiLU, with no normalization (left) and BN (right).

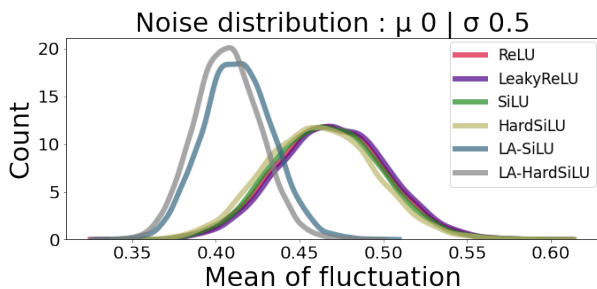


Figure 4: Distribution of activation output fluctuation.

mean of zero and a variance of  $0.5^2$ , and another with a mean of one and a variance of  $0.5^2$ .

Figure 4 shows the distribution of the activation fluctuation with a noise distribution. Although the fluctuation distribution of the activation input was similar (see Appendix K), LayerAct functions have a significantly smaller mean and variance of activation fluctuation among the samples than any other ElementAct function in all cases. The decrease in variance is remarkable, showing that LayerAct functions are robust for all samples. Moreover, the ElementAct functions that ensure a zero-like activation mean with one-sided saturation such as SiLU or HardSiLU showed slightly larger activation fluctuations than those of ReLU or LReLU when the noise had a large mean. However, LayerAct functions maintained lower fluctuations in both cases.

**Zero-like Activation Mean** Figure 5 demonstrates the distribution of the activation output means of the single-layer network trained on the MNIST dataset at the epoch 40. The distributions did not change after the epoch 40. LayerAct functions maintain a zero-like activation mean for all epochs. Our experimental results indicate that LayerAct allows similar (before epoch 20) or larger (after epoch 40) negative outputs compared to other ElementAct functions. Thus, LA-SiLU and LA-HardSiLU can achieve a more zero-like activation mean than other activation functions.

### Classification Performance

We demonstrate the classification performance of LayerAct on CIFAR10, ImageNet (Russakovsky et al. 2015), and a medical image dataset. We used ResNet (He et al. 2016) as the network for our experiments on the three benchmark datasets. In our experiments on CIFAR10 and Im-

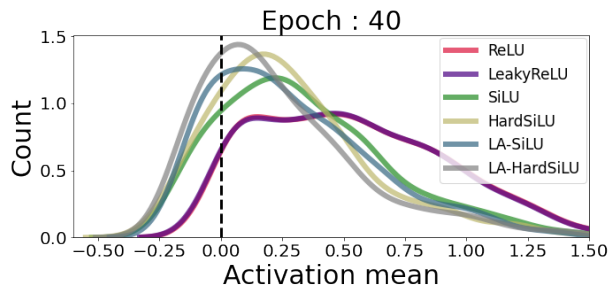


Figure 5: Distribution of the activation output means of the elements in a trained network on MNIST at epoch 40.

geNet, we utilized BN. We compared LayerAct with ReLU, LReLU, PReLU, SiLU, HardSiLU, Mish (Misra 2020), GELU (Hendrycks and Gimpel 2023), and ELU (Clevert, Unterthiner, and Hochreiter 2016). In the tables, The best results are underlined and bolded, and the second best are bolded. In the main manuscript, we present the results of ResNet20 on CIFAR10 and ResNet50 and ResNet101 on ImageNet. For more experimental results, including on CIFAR100, see Appendix J.

**On CIFAR10 and CIFAR10-C** The column named clean of Table 2 presents the classification performance of ResNet20 with both LayerAct functions and ElementAct functions, benchmarked on the clean CIFAR10. We report the mean accuracy over 30 runs. LA-SiLU achieved the best performance among the activation functions. In other experiments, with ResNet32 and ResNet44 on clean CIFAR10 (Appendix J), networks with GELU achieved better results in two cases: ResNet32 on CIFAR10 and ResNet44 on CIFAR100. In the remaining combinations of networks and datasets, LA-SiLU outperformed in a significant majority of cases, especially in 39 out of 48 cases according to the  $p$ -value from a T-test or a Wilcoxon signed-rank test, indicating statistical significance.

To verify the robustness of LayerAct functions, we evaluated their classification performance on CIFAR10-C. The columns other except clean in Table 2 demonstrates the experimental results. The networks with LayerAct functions achieved remarkable performance compared to those with ElementAct functions. Specifically, LA-SiLU and LA-HardSiLU statistically outperformed other ElementAct functions in 46 out of 48 cases for each, according to the  $p$ -value from a T-test or a Wilcoxon signed-rank test. This shows that LayerAct functions exhibit greater robustness to intense noise compared to other functions. Furthermore, the experimental results on ResNets without a normalization method reveal that LA-SiLU can maintain its robustness when inputs are not excessively large.

**On ImageNet** Table 3 shows the performance of ResNet50 and ResNet101 with LayerAct functions and other ElementAct functions for comparison with clean and noisy ImageNet datasets. For the column named "clean," we report the accuracy of 10-crop testing on the validation dataset. We

Activation	CIFAR10			CIFAR10-C			
	Clean	Total	Noise	Blur	Digital	Weather	Extra
ReLU	91.3 (0.045)	68.8 (1.735)	50.3 (5.967)	65.2 (2.294)	72.7 (0.948)	78.6 (0.523)	72.6 (1.471)
LReLU	91.3 (0.069)	68.7 (1.595)	49.9 (5.175)	65.3 (2.234)	72.7 (0.801)	78.4 (0.481)	72.5 (1.464)
PReLU	90.8 (0.054)	67.9 (2.010)	50.0 (6.180)	64.0 (1.990)	71.9 (1.700)	77.3 (0.669)	71.7 (1.787)
SiLU	<b>91.5</b> (0.042)	69.0 (1.225)	50.2 (3.131)	65.6 (1.815)	72.5 (0.763)	78.9 (0.492)	73.0 (1.015)
HardSiLU	91.1 (0.052)	68.5 (1.453)	49.7 (5.605)	65.2 (1.971)	72.0 (0.652)	78.2 (0.418)	72.8 (1.191)
MISH	91.5 (0.053)	69.0 (1.324)	50.0 (4.568)	65.7 (1.720)	72.6 (0.627)	78.9 (0.401)	72.9 (1.267)
GELU	<b>91.5</b> (0.035)	68.6 (1.290)	49.8 (3.318)	64.9 (2.311)	72.5 (0.729)	78.7 (0.276)	72.6 (1.276)
ELU	91.0 (0.030)	68.7 (1.363)	48.3 (5.193)	66.5 (1.842)	72.3 (0.605)	78.8 (0.355)	72.5 (1.220)
LA-SiLU	<b>91.6</b> (0.027)	<b>70.4</b> (1.392)	<b>51.8</b> (3.527)	<b>67.5</b> (2.155)	<b>74.0</b> (0.948)	<b>79.9</b> (0.559)	<b>74.4</b> (1.014)
LA-HardSiLU	91.2 (0.042)	<b>70.3</b> (1.384)	<b>52.2</b> (5.707)	<b>67.5</b> (1.238)	<b>73.5</b> (0.836)	<b>79.5</b> (0.501)	<b>74.3</b> (1.127)

Table 2: Classification performance of ResNet20 on the CIFAR10 and CIFAR10-C. We present mean and (variance).

Model	Activation	ImageNet			ImageNet-C			
		Clean	Total	Noise	Blur	Digital	Weather	Extra
ResNet50	ReLU	77.71	<b>43.75</b>	<b>34.40</b>	36.85	<b>48.37</b>	47.18	49.60
ResNet50	LReLU	77.83	43.24	32.87	36.33	48.00	47.03	49.38
ResNet50	PReLU	74.99	36.77	23.28	32.27	43.29	39.56	42.05
ResNet50	SiLU	77.85	42.31	29.74	35.94	46.59	47.36	48.77
ResNet50	HardSiLU	76.30	40.56	26.21	35.14	46.01	45.23	46.63
ResNet50	Mish	77.41	42.57	31.24	36.60	46.73	46.83	48.64
ResNet50	GELU	78.01	40.71	27.82	35.35	45.34	44.52	47.28
ResNet50	LA-SiLU	<b>78.62</b>	<b>45.29</b>	<b>36.16</b>	<b>37.66</b>	<b>50.31</b>	<b>48.33</b>	<b>51.71</b>
ResNet50	LA-HardSiLU	<b>78.24</b>	43.63	32.21	<b>37.57</b>	47.69	<b>47.88</b>	<b>49.93</b>
ResNet101	ReLU	<b>79.24</b>	46.7	36.29	39.75	52.16	49.93	52.78
ResNet101	LA-SiLU	79.12	<b>47.87</b>	<b>39.62</b>	<b>39.85</b>	<b>52.82</b>	<b>50.84</b>	<b>54.16</b>

Table 3: Classification performance of ResNet50 and ResNet101 on the clean and noisy ImageNet.

Activation	U-net	Unet++ w/o DSV	Unet++ w DSV
ReLU	84.71	84.94	84.92
SiLU	84.87	85.15	85.01
LA-SiLU	<b>85.13</b>	<b>85.27</b>	<b>85.05</b>

Model	ReLU		SiLU		LA-SiLU	
	Nat	Adv	Nat	Adv	Nat	Adv
RN18	81.79	82.73	83.28	82.93	<b>83.64</b>	<b>84.14</b>

Table 4: Additional experiments on medical image segmentation (upper) and adversarial robustness (lower).

used the out-of-distribution benchmark dataset, ImageNet-C (Hendrycks and Dietterich 2019), which has the same corruptions as CIFAR-C datasets. The networks with LayerAct functions outperformed those with other activation functions on all datasets. The ResNet50 with LayerAct functions, even with LA-HardSiLU which showed worse performance on the clean CIFAR10 datasets compared to SiLU or LReLU, outperformed other activation functions on clean ImageNet. Based on these results, we trained deeper networks, ResNet101, utilizing ReLU and LA-SiLU as activations. LA-SiLU maintained its superior robustness.

**Additional Experiments** To evaluate LayerAct’s effectiveness, we conducted additional experiments on a nuclei

image dataset (Goodman et al. 2018) for segmentation and on CIFAR10 to verify adversarial robustness. Table 4 shows that networks with LA-SiLU outperform those with ReLU or SiLU in both tasks. Results from segmentation tasks with U-Net (Olaf Ronneberger 2015) and UNet++ (Zhou et al. 2018) show LayerAct’s potential across different architectures for image tasks. The experimental results on adversarial robustness with ResNet18 (RN18) further underscore LayerAct’s robustness. For the detail, see Appendices L and M for experiments on medical image and adversarial robustness, respectively.

## Conclusion

In this work, we identified the fundamental limitation of ElementAct in robustness and demonstrated that layer-direction normalization has the potential to enhance the robustness of activation. Inspired by our investigation, we have developed LayerAct mechanism and functions that not only enhance robustness compared to existing activation functions but also resolve the trade-off problem. Moreover, unlike LN, LayerAct does not reduce the performance of CNNs when utilized with BN on clean dataset. Experimental results on benchmark datasets show that LayerAct functions preserve essential activation properties and provide robust performance on both clean and noisy datasets, underscoring their utility and effectiveness in advanced CNN architectures.

## Acknowledgements

This research was partly supported by the Basic Science Research Program through the National Research Foundation of Korea (NRF), funded by the Ministry of Education (RS-2024-00463188) and the Ministry of Science and ICT (RS-2024-00458720), as well as by the Institute of Information & Communications Technology Planning & Evaluation (IITP) grants funded by the Korean government (MSIT) (No.RS-2024-00439932, SW Starlab; No.RS-2020-II201336, Artificial Intelligence Graduate School Program - UNIST; No.RS-2021-II212068, Artificial Intelligence Innovation Hub; No.RS-2024-00443780, Development of Foundation Models for Bioelectrical Signal Data and Validation of Their Clinical Applications: A Noise-and-Variability Robust, Generalizable Self-Supervised Learning Approach).

## References

- Ba, J. L.; Kiros, J. R.; and Hinton, G. E. 2016. Layer Normalization. arXiv:1607.06450.
- Clevert, D.-A.; Unterthiner, T.; and Hochreiter, S. 2016. Fast and accurate deep network learning by exponential linear units (elus). In *International Conference on Learning Representations (ICLR)*.
- Elfwing, S.; Uchibe, E.; and Doya, K. 2018. Sigmoid-weighted linear units for neural network function approximation in reinforcement learning. *Neural Networks*, 107: 3–11.
- Glorot, X.; Bordes, A.; and Bengio, Y. 2011. Deep Sparse Rectifier Neural Networks. In *International Conference on Artificial Intelligence and Statistics (AISTATS)*, volume 15, 315–323.
- Goodman, A.; Carpenter, A.; Park, E.; jleflman nvidia; Josette.BoozAllen; Kyle; Maggie; Nilofer; Sedivec, P.; and Cukierski, W. 2018. 2018 Data Science Bowl. <https://kaggle.com/competitions/data-science-bowl-2018>. Accessed: 2024-12-17.
- He, K.; Zhang, X.; Ren, S.; and Sun, J. 2015. Delving Deep into Rectifiers: Surpassing Human-Level Performance on ImageNet Classification. In *Proceedings of the IEEE International Conference on Computer Vision (ICCV)*.
- He, K.; Zhang, X.; Ren, S.; and Sun, J. 2016. Deep Residual Learning for Image Recognition. In *Proceedings of the IEEE Conference on Computer Vision and Pattern Recognition (CVPR)*.
- Hendrycks, D.; and Dietterich, T. 2019. Benchmarking Neural Network Robustness to Common Corruptions and Perturbations. In *International Conference on Learning Representations (ICLR)*.
- Hendrycks, D.; and Gimpel, K. 2023. Gaussian Error Linear Units (GELUs). arXiv:1606.08415.
- Howard, A.; Sandler, M.; Chu, G.; Chen, L.-C.; Chen, B.; Tan, M.; Wang, W.; Zhu, Y.; Pang, R.; Vasudevan, V.; Le, Q. V.; and Adam, H. 2019. Searching for MobileNetV3. In *Proceedings of the IEEE/CVF International Conference on Computer Vision (ICCV)*.
- Huang, L.; Yang, D.; Lang, B.; and Deng, J. 2018. Decorrelated Batch Normalization. In *Proceedings of the IEEE Conference on Computer Vision and Pattern Recognition (CVPR)*.
- Ioffe, S.; and Szegedy, C. 2015. Batch Normalization: Accelerating Deep Network Training by Reducing Internal Covariate Shift. In *International Conference on Machine Learning (ICML)*, volume 37, 448–456. PMLR.
- Krizhevsky, A. 2009. *Learning Multiple Layers of Features from Tiny Images*. Ph.D. thesis, University of Toronto.
- Krizhevsky, A.; Sutskever, I.; and Hinton, G. E. 2012. ImageNet Classification with Deep Convolutional Neural Networks. In *Advances in Neural Information Processing Systems (NeurIPS)*, volume 25.
- Labatie, A.; Masters, D.; Eaton-Rosen, Z.; and Luschi, C. 2021. Proxy-Normalizing Activations to Match Batch Normalization while Removing Batch Dependence. In *Advances in Neural Information Processing Systems (NeurIPS)*, volume 34, 16990–17006. Curran Associates, Inc.
- Lee, C.-Y.; Xie, S.; Gallagher, P.; Zhang, Z.; and Tu, Z. 2015. Deeply-Supervised Nets. In *AISTATS*, volume 38, 562–570.
- Liang, S.; Huang, Z.; Liang, M.; and Yang, H. 2020. Instance enhancement batch normalization: An adaptive regulator of batch noise. In *AAAI*, volume 34, 4819–4827.
- Lubana, E. S.; Dick, R.; and Tanaka, H. 2021. Beyond BatchNorm: Towards a Unified Understanding of Normalization in Deep Learning. In *Advances in Neural Information Processing Systems (NeurIPS)*, volume 34, 4778–4791. Curran Associates, Inc.
- Luo, P.; Zhang, R.; Ren, J.; Peng, Z.; and Li, J. 2019. Switchable normalization for learning-to-normalize deep representation. *IEEE transactions on pattern analysis and machine intelligence*, 43(2): 712–728.
- Maas, A. L.; Hannun, A. Y.; Ng, A. Y.; et al. 2013. Rectifier nonlinearities improve neural network acoustic models. In *International Conference on Machine Learning (ICML)*, volume 30, 3.
- Misra, D. 2020. Mish: A Self Regularized Non-Monotonic Activation Function. arXiv:1908.08681.
- Nair, V.; and Hinton, G. E. 2010. Rectified linear units improve restricted boltzmann machines. In *International Conference on Machine Learning (ICML)*, 807–814.
- Olaf Ronneberger, T. B., Philipp Fischer. 2015. U-net: Convolutional networks for biomedical image segmentation. In *Medical Image Computing and Computer-Assisted Intervention (MICCAI)*, 234–241.
- Paszke, A.; Gross, S.; Massa, F.; Lerer, A.; Bradbury, J.; Chanan, G.; Killeen, T.; Lin, Z.; Gimelshein, N.; Antiga, L.; Desmaison, A.; Kopf, A.; Yang, E.; DeVito, Z.; Raison, M.; Tejani, A.; Chilamkurthy, S.; Steiner, B.; Fang, L.; Bai, J.; and Chintala, S. 2019. PyTorch: An Imperative Style, High-Performance Deep Learning Library. In *Advances in Neural Information Processing Systems (NeurIPS)*, volume 32.

- Qiu, S.; Xu, X.; and Cai, B. 2018. FReLU: Flexible Rectified Linear Units for Improving Convolutional Neural Networks. In *International Conference on Pattern Recognition (ICPR)*, 1223–1228.
- Ramachandran, P.; Zoph, B.; and Le, Q. V. 2018. Searching for activation functions. In *International Conference on Learning Representations (ICLR) Workshop*.
- Russakovsky, O.; Deng, J.; Su, H.; Krause, J.; Satheesh, S.; Ma, S.; Huang, Z.; Karpathy, A.; Khosla, A.; Bernstein, M.; et al. 2015. Imagenet large scale visual recognition challenge. *International Journal of Computer Vision (IJCV)*, 115(3): 211–252.
- Tenenbaum, J. B.; de Silva, V.; and Langford, J. C. 2000. A Global Geometric Framework for Nonlinear Dimensionality Reduction. *Science*, 290(5500): 2319–2323.
- Ulyanov, D.; Vedaldi, A.; and Lempitsky, V. 2017. Instance Normalization: The Missing Ingredient for Fast Stylization. arXiv:1607.08022.
- Zhou, N.; Wang, N.; Liu, D.; Zhou, D.; and Gao, X. 2023. Enhancing Robust Representation in Adversarial Training: Alignment and Exclusion Criteria. arXiv:2310.03358.
- Zhou, Z.; Rahman Siddiquee, M. M.; Tajbakhsh, N.; and Liang, J. 2018. Unet++: A nested u-net architecture for medical image segmentation. In *Deep Learning in Medical Image Analysis and Multimodal Learning for Clinical Decision Support (DLMIA)*, 3–11.

## A. Important Properties of Activation

One-side saturation and zero-like activation mean stand out as crucial properties of activation for effective and efficient network training. Activation functions that exhibit one-side saturation, such as the ReLU, are favored within deep networks for their potential to provide more informative signal propagation during the backward pass by allowing for larger derivatives (Glorot, Bordes, and Bengio 2011). Furthermore, the presence of a saturation state contributes to robustness against input shifts, maintaining consistent activation outputs for elements in this state and thereby stabilizing network training (Clevert, Unterthiner, and Hochreiter 2016; Qiu, Xu, and Cai 2018).

Achieving a zero-like activation mean is another important property of activation functions, facilitating efficient network training. The activation mean refers to the average activation output of an individual element across samples. Functions such as the Exponential Linear Unit (ELU) (Clevert, Unterthiner, and Hochreiter 2016) and Parametric ReLU (PReLU) (He et al. 2015) push the activation mean toward zero by allowing negative outputs. Activation functions with this property can correct the bias shift that occurs between layers and lead to efficient network training (Clevert, Unterthiner, and Hochreiter 2016; Qiu, Xu, and Cai 2018).

The activation output of the  $i^{\text{th}}$  unit of  $m^{\text{th}}$  sample ( $m \in \{1, 2, \dots, M\}$ ) is defined as  $a_{m,i} = f(y_{m,i})$ , where  $f$ ,  $y_{m,i}$ , and  $M$  are activation function, the  $i^{\text{th}}$  activation input of the  $m^{\text{th}}$  sample, and the number of samples in the batch, respectively. Ideally, a “zero-like activation mean” occurs when the activation mean of a single unit,  $a_i$ , approximates zero across the samples. Mathematically, this can be represented as:

$$\frac{1}{M} \sum_{m=1}^M a_{m,i} \approx 0.$$

However, approximating the activation mean to zero is challenging for activation functions that saturate at (large) negative outputs, such as ELU, SiLU, or FReLU. Due to this saturation, previous studies have defined the “zero-like activation mean” property of an activation function as its ability to “push” the activation mean towards zero. In mathematical terms, this can be presented as  $|\mu_{a_i}| \ll c$ , where  $c$  is a small positive constant (Clevert, Unterthiner, and Hochreiter 2016; Qiu, Xu, and Cai 2018).

## B. Detailed Derivation Process of Activation Fluctuation with LN

In this section, we present the detailed derivation process of the equations in Definition 4 in the main manuscript as follows:

$$\begin{aligned} \|f(\hat{n}) - f(n)\| &= \sum_{i=1}^D |\hat{n}_i s(\hat{n}_i) - n_i s(n_i)| \\ &= \sum_{i=1}^D \left| \frac{\hat{y}_i + \epsilon_i - \mu_y - \mu_\epsilon}{\sqrt{\sigma_y^2 + \sigma_\epsilon^2 + \alpha}} s(\hat{n}_i) - \frac{y_i - \mu_y}{\sqrt{\sigma_y^2 + \alpha}} s(n_i) \right| \\ &\approx \sum_{i=1}^D \left| n_i (s(\hat{n}_i) - s(n_i)) + \frac{(\epsilon - \mu_\epsilon) s(\hat{n}_i)}{\sqrt{\sigma_y^2 + \alpha}} \right| \\ &\leq \sum_{i=1}^D \left( |n_i| \cdot |s(\hat{n}_i) - s(n_i)| + \frac{|\epsilon - \mu_\epsilon| \cdot s(\hat{n}_i)}{\sqrt{\sigma_y^2 + \alpha}} \right), \end{aligned}$$

where  $\sqrt{\sigma_y^2 + \alpha + \sigma_\epsilon^2} \approx \sqrt{\sigma_y^2 + \alpha} > 1$  when  $\sigma_y \gg \sigma_\epsilon$  and  $\alpha$  is sufficiently large.

## C. Difference between LayerAct and Activation with LN

In this section, we provide detailed comparison between the activation outputs of LayerAct and those of element-level activation functions paired with LN. When a LN layer is placed right before an activation layer, the  $i^{\text{th}}$  activation output is  $a_i = n_i^{LN} s(n_i^{LN})$ , where  $n_i^{LN}$  is the  $i^{\text{th}}$  normalized output of LN. Conversely, the  $i^{\text{th}}$  activation output of a LayerAct function is  $a_i = y_i s(n_i)$ , as defined in Equation 12 in the main manuscript.

The critical distinction between activation with LN and LayerAct lies in the preservation of input mean and variance statistical information in the activation output. *LayerAct can preserve the statistical information, but activation with LN cannot.* With LN, the activation function takes a normalized input in layer-direction, resulting in activation outputs that exhibit similar mean and variance across samples (as shown in the activation output equation for LN above). This homogenization of statistical information across samples, a characteristic of LN, is a reason why BN often outperforms LN in non-sequential models such as CNNs (Labatie et al. 2021; Lubana, Dick, and Tanaka 2021). In the main manuscript, we demonstrated that this homogeneity limitation of LN leads the representation of the samples with different labels to be similar (see Figure 1 in the main manuscript).

LayerAct, on the other hand, produces more distinguishable activation outputs between samples by preserving statistical variation between samples. This is due to the fact that only the activation scale function of LayerAct uses the layer-normalized input, not the LayerAct function itself (as shown in Equation 12 in the main manuscript). Based on this unique output of LayerAct, networks with LayerAct can produce much more distinguishable representation of samples compared to those with activation and LN (see Figure 3 in the main manuscript).

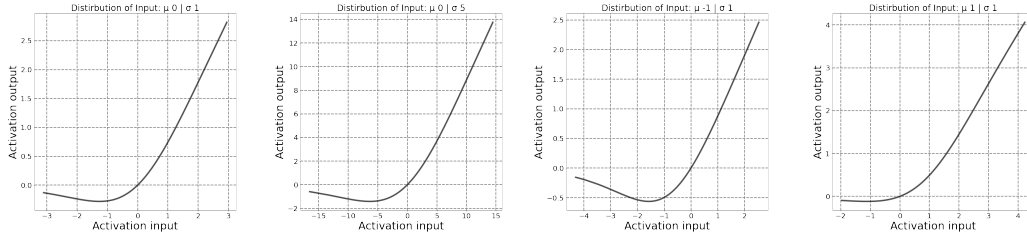


Figure 6: LA-SiLU with different mean and variance values in the input. The distribution of the activation input is: (1)  $\mu_y = 0, \sigma_y = 1$ , (2)  $\mu_y = 0, \sigma_y = 5$ , (3)  $\mu_y = -5, \sigma_y = 1$ , and (4)  $\mu_y = 5, \sigma_y = 1$  from the left to right.

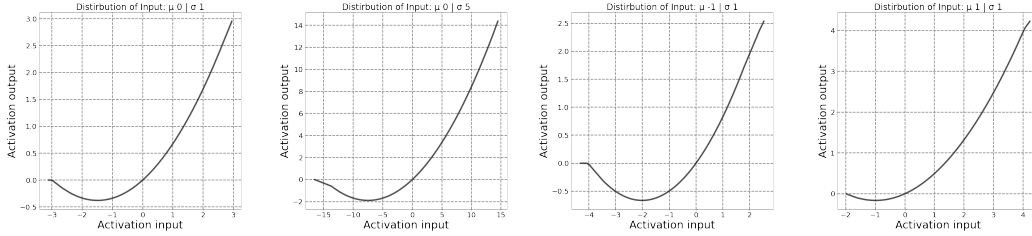


Figure 7: LA-HardSiLU with different mean and variance values in the input. The distribution of the activation input is: (1)  $\mu_y = 0, \sigma_y = 1$ , (2)  $\mu_y = 0, \sigma_y = 5$ , (3)  $\mu_y = -5, \sigma_y = 1$ , and (4)  $\mu_y = 5, \sigma_y = 1$  from the left to right.

## D. Activation Output of LayerAct Functions

In this section, we provide detailed comparison between the activation outputs of LayerAct and those of element-level activation functions paired with LN. When a LN layer is placed right before an activation layer, the  $i^{th}$  activation output is  $a_i = n_i^{LN} s(n_i^{LN})$ , where  $n_i^{LN}$  is the  $i^{th}$  normalized output of LN. Conversely, the  $i^{th}$  activation output of a LayerAct function is  $a_i = y_i s(n_i)$ , as defined in Equation 12 in the main manuscript.

The critical distinction between activation with LN and LayerAct lies in the preservation of input mean and variance statistical information in the activation output. *LayerAct can preserve the statistical information, but activation with LN cannot.* With LN, the activation function takes a normalized input in layer-direction, resulting in activation outputs that exhibit similar mean and variance across samples (as shown in the activation output equation for LN above). This homogenization of statistical information across samples, a characteristic of LN,

is a reason why BN often outperforms LN in non-sequential models such as CNNs (Labatie et al. 2021; Lubana, Dick, and Tanaka 2021).

LayerAct, on the other hand, produces more distinguishable activation outputs between samples by preserving statistical variation between samples. This is due to the fact that only the activation scale function of LayerAct uses the layer-normalized input, not the LayerAct function itself (as shown in Equation 12 in the main manuscript).

### E. Trade-off between Two Properties

A fundamental trade-off exists between the important properties of activation, one-side saturation and zero-like mean activation. Activation functions that have a saturation state typically limit negative outputs, consequently driving the activation mean away from zero. On the other hand, to achieve a zero-like activation mean, certain functions like PReLU allow large negative outputs. However, functions with this allowance are not robust due to the absence of saturation.

To address this trade-off issue, various activation functions, such as Sigmoid Linear Unit (SiLU, also known as SWISH) (Elfwing, Uchibe, and Doya 2018; Ramachandran, Zoph, and Le 2018), Gaussian Error Linear Unit (GELU) (Hendrycks and Gimpel 2023), and Mish (Misra 2020), saturate the large negative outputs only. These activation functions can achieve a zero-like activation mean with small negative outputs. However, a trade-off still exists because the restriction of negative outputs, designed to ensure saturation, prevents the allowance of large negative outputs, thereby restraining the mean of activation from being more zero-like.

*Additionally, this trade-off cannot be addressed by LN.* Even when a LN layer is placed before the activation layer, the large negative output is restricted with element-level activation. Therefore, mitigating the trade-off between activation properties is a distinct benefit of LayerAct functions that element-level activation functions cannot attain.

### F. Experimental Setting

We implemented LayerAct functions and networks for experiment with PyTorch (Paszke et al. 2019). All networks used in our experiments were trained on NVIDIA A100. We used multiple devices to train the networks on ImageNet, and a single device for the other experiments. The versions of Python and the packages were (1) Python 3.9.12, (2) numpy 1.19.5 (3) PyTorch 1.11.0, and (4) torchvision 0.12.0. We used cross entropy loss functions for all the experiments. The random seeds of the experiments were  $11 \times i$  where  $i \in \{1, 2, \dots, 30\}$  on CIFAR10 and CIFAR100 and 11 on ImageNet.

To train networks on MNIST for experimental analysis, we applied batch gradient descent for 80 epochs with the weight decay and momentum fixed to 0.0001 and 0.9, respectively. The learning rate started from 0.01, and was multiplied 0.1 at epochs 40 and 60 as scheduled. We used ResNet (He et al. 2016) with BN right before activation for experiments on CIFAR10, CIFAR100 and ImageNet. We initialized the weights following the methods proposed by He et al. (He et al. 2015). For all experiments, the weight decay, momentum, and initial learning rate were 0.0001, 0.9 and 0.1, respectively.

For CIFAR10 and CIFAR100, we trained ResNet20, ResNet32, and ResNet44 with a basic block using the stochastic gradient descent with a batch size of 128 for about 64000 iterations. We randomly selected 10% of the training dataset as the validation set. The learning rate was scheduled to decrease by the factor of 10 at 32000 and 48000 iterations. For the data augmentation of CIFAR10 and CIFAR100, we followed (Lee et al. 2015). We rescaled the data between 0 and 1, padded 4 pixels on each side, and randomly sampled a  $32 \times 32$  crop from the padded image or its horizontal flip. The data was normalized after augmentation. For testing, we did not apply data augmentation, only normalized the data. The hyper-parameter  $\alpha$  of LayerAct functions for the experiments was set to 0.00001.

For the experiment with ImageNet, we trained ResNet50 and ResNet101 with the bottleneck block using stochastic gradient descent, and the batch size was 256 for about 600000 iterations. The learning rate was scheduled to decrease by a factor of 10 at 180000, 360000, and 540000 iterations. For the data augmentation on ImageNet, we rescaled the data between 0 and 1, resized it to  $224 \times 224$ , and randomly sampled a  $224 \times 224$  crop from an image or its horizontal flip (Krizhevsky, Sutskever, and Hinton 2012). We normalized the data after data augmentation. For testing, we resized the data to be  $256 \times 256$  and applied 10-crop. Afterward, the data was normalized. To ensure stable learning, we set the hyper-parameter  $\alpha$  of LayerAct functions to 0.1 which is larger than those for CIFAR10 and CIFAR100.

For the reproducibility, we have attached the code that used for the experiments in supplementary materials.

## G. Relationship between LayerAct and BN

In our main manuscript, we emphasized the importance of selecting an appropriate normalization method for employing LayerAct functions effectively. This section delves into the relationship between LayerAct and BN, the most dominant normalization method for CNNs. In this section, our objective is to discuss the benefits of BN in CNNs and demonstrate how LayerAct functions collaborate well with BN, in contrast to LN.

BN operates along three dimensions, batch, height, and width, particularly for image datasets, where the input matrix  $y \in \mathbb{R}^{B \times C \times H \times W}$ . To simplify, we consider a flattened dimension that combines height and width, denoted by size  $D$ . The mean, variance, and output of BN are then defined as follows:

$$\mu_j^{BN} = \frac{1}{BD} \sum_{i=1}^B \sum_{k=1}^D y_{i,j,k}, \quad (17)$$

$$\sigma_j^{BN} = \frac{1}{BD} \sum_{i=1}^B \sum_{k=1}^D (y_{i,j,k} - \mu_j^{BN}), \quad (18)$$

$$n_{i,j,k}^{BN} = \gamma_j \cdot \frac{y_{i,j,k} - \mu_j^{BN}}{\sqrt{\sigma_j^{BN^2} + \alpha}} + \beta_j. \quad (19)$$

BN enjoys the common advantages of normalization methods, re-scaling and re-centering operations that significantly enhance the efficiency and effectiveness of network training, promote stable training, and allow the use of a larger learning rate (Lubana, Dick, and Tanaka 2021; Labatie et al. 2021; Ioffe and Szegedy 2015).

Additionally, BN offers the unique benefit of avoiding channel collapse, a phenomenon where a channel exhibits a linear activation (i.e. a channel loses its non-linear activation), leading to inefficient network training (Labatie et al. 2021). For instance, when a channel’s activation inputs are consistently positive or negative across all samples, the activation output of a ReLU layer becomes linear,  $a = y$  or  $a = 0$ , respectively. BN addresses this by normalizing across the batch dimension, ensuring a diverse distribution of channel activations among samples. Moreover, it does not have the homogenization issue present in LN.

When utilized with LayerAct, BN does not compromise the benefits of LayerAct because they operate on different normalization dimensions. Given that the output of LayerAct functions is the product of the activation input (i.e. the normalization output) and the activation scale, BN’s benefits extend to the activation output, enhancing overall network performance as when utilized with element-level activation function. Therefore, utilizing LayerAct with BN preserves the advantages of both, enhancing the efficiency of network training and robustness of network inference.

In summary, the choice of normalization method for CNNs with LayerAct functions should be made carefully, taking into account the interplay between LayerAct and the normalization. While LN may diminish LayerAct’s benefits, as discussed in Appendix , BN, with its beneficial properties, would be a suitable choice for CNNs with LayerAct functions on image datasets.

## H. LayerAct with no normalization or LN

In this section, we explore the cases when LA-SiLU is utilized with LN. For the further investigation, we first examine the relationship between LN and LayerAct, subsequently presenting experimental results on CIFAR datasets for two scenarios: (1) networks without any normalization methods, and (2) networks with LN. ReLU and SiLU were selected as baseline element-level activation functions, with ReLU being the most popular choice for CNNs, and SiLU being as the corresponding element-level activation function of LA-SiLU.

For the networks incorporating LN, the normalization output of a LN layer is expressed as  $n^{\hat{LN}} = \gamma \cdot \frac{y - \mu_y^2}{\sqrt{\sigma_y^2 + \alpha}} + \beta$ . This equation results in the output of SiLU  $n^{\hat{LN}} s(n^{\hat{LN}})$  and LA-SiLU  $n^{\hat{LN}} s(n)$  becoming similar. When the learnable parameter  $\gamma$  and  $\beta$  are 1 and 0, respectively, the outputs  $n^{\hat{LN}} s(n^{\hat{LN}})$  and  $n^{\hat{LN}} s(n)$  become identical, nullifying any distinct advantage offered by the LayerAct mechanism. Thus, the more the output of

Table 5: Classification performance on CIFAR and CIFAR-C datasets without a normalization method. C10 and C100 denotes CIFAR10 and CIFAR100, respectively.

Data	Model	Activation	CIFAR			CIFAR-C			
			Clean	Total	Noise	Blur	Digital	Weather	Extra
C10	ResNet20	ReLU	88.51	67.43	53.27	62.12	70.93	75.91	71.38
C10	ResNet20	SiLU	88.29	68.94	54.66	<b>65.84</b>	71.6	76.54	72.48
C10	ResNet20	LA-SiLU	<b>88.95</b>	<b>69.36</b>	<b>54.71</b>	<b>65.58</b>	<b>71.93</b>	<b>77.59</b>	<b>73.34</b>
C10	ResNet32	ReLU	<b>89.56</b>	68.94	54.48	63.90	72.45	77.52	72.73
C10	ResNet32	SiLU	46.51	38.69	33.21	37.52	39.62	41.6	40.11
C10	ResNet32	LA-SiLU	89.12	<b>70.59</b>	<b>56.29</b>	<b>66.81</b>	<b>73.11</b>	<b>78.94</b>	<b>74.22</b>
C10	ResNet44	ReLU	<b>90.03</b>	69.97	55.75	65.08	73.38	78.45	73.62
C10	ResNet44	SiLU	15.25	14.18	13.5	14.01	14.26	14.55	14.39
C10	ResNet44	LA-SiLU	88.77	<b>71.65</b>	<b>58.15</b>	<b>68.32</b>	<b>74.01</b>	<b>79.49</b>	<b>74.88</b>
C100	ResNet20	ReLU	59.46	37.69	21.17	38.76	41.36	44.15	38.89
C100	ResNet20	SiLU	59.74	40.39	24.21	42.72	43.51	46.45	41.01
C100	ResNet20	LA-SiLU	<b>61.01</b>	<b>42.44</b>	<b>26.07</b>	<b>44.50</b>	<b>45.74</b>	<b>48.8</b>	<b>42.98</b>
C100	ResNet32	ReLU	<b>60.71</b>	39.56	23.05	40.78	43.23	45.93	40.67
C100	ResNet32	SiLU	20.36	14.99	10.05	16.27	15.89	16.47	15.02
C100	ResNet32	LA-SiLU	60.08	<b>44.01</b>	<b>28.77</b>	<b>46.73</b>	<b>47.02</b>	<b>49.51</b>	<b>44.19</b>
C100	ResNet44	ReLU	<b>61.59</b>	40.88	24.57	42.08	44.60	47.16	41.90
C100	ResNet44	SiLU	2.91	2.43	1.97	2.58	2.53	2.54	2.42
C100	ResNet44	LA-SiLU	60.30	<b>44.26</b>	<b>29.22</b>	<b>46.74</b>	<b>47.45</b>	<b>49.65</b>	<b>44.50</b>

the LN layer approximates the normalized input of LayerAct’s activation scale function (i.e., the more gain and bias approximate to 1 and 0, respectively), the more the benefits of LayerAct are reduced.

Nevertheless, the benefits of LayerAct functions, addressing the trade-off between two important activation properties and potentially exhibiting lower variance in robustness across samples, can still be partially retained when combined with LN that the learnable parameters  $\gamma$  and  $\beta$  are far from 1 and 0, respectively. This is because the layer-direction normalized input of LayerAct’s activation scale function does not utilize an affine function. By not utilizing an affine function, we can ensure that  $\|s(\hat{n})\|$  of LayerAct functions remains small enough for robustness. When an affine function is used, the mean of the normalized vector  $n$  can become large if the parameter  $\beta$  is large. Such large  $n$  leads to a large  $\|s(\hat{n})\|$ , which does not ensure robustness.

Additionally, LayerAct functions can allow a larger negative output compared to element-level activation functions, as they do not restrict large negative outputs. Furthermore, the robustness benefit of LayerAct becomes significant when the normalized outputs of LN (i.e. activation input) are mostly outside the saturation state.

To investigate this, we conducted experiments on ResNets both without normalization and with LN. We followed the same experimental setting of the experiments in our main manuscript. The results reported in the tables are the average accuracies over 30 runs, each with different seeds for weight initialization.

Table 5 presents the performance of ResNets without any normalization methods on both clean and noisy CIFAR datasets, with a learning rate set at 0.01 for stable training. The results demonstrate that networks with LA-SiLU outperformed those with ReLU and SiLU on noisy datasets. This indicates that the robustness of LayerAct functions is independent from the presence of normalization layers. Additionally, while networks with SiLU, the corresponding element-level activation function, experienced training instability and often exploded, those with LA-SiLU maintained stable training. This suggests that the LayerAct mechanism can contribute to more stable network training. However, in deeper networks such as ResNet32 and ResNet44, the performance with ReLU surpassed those with LA-SiLU. This outcome may be because of the more complex representation of LA-SiLU’s output, pointing towards the necessity of a normalization layer to mitigate potential overfitting issues.

Table 6 demonstrates the performance of ResNets with LN on both clean and noisy CIFAR10 and CIFAR100 datasets. It validated our concerns about the relationship between LN and LayerAct. On noisy CIFAR100,

Table 6: Classification performance on CIFAR and CIFAR-C datasets with LN. C10 and C100 denote CIFAR10 and CIFAR100, respectively.

Data	Model	Activation	CIFAR			CIFAR-C			
			Clean	Total	Noise	Blur	Digital	Weather	Extra
C10	ResNet20	ReLU	88.24	73.77	62.05	71.26	76.48	79.69	76.46
C10	ResNet20	SiLU	87.53	74.3	63.32	71.74	77.33	79.77	76.58
C10	ResNet20	LA-SiLU	<b>88.52</b>	<b>75.31</b>	<b>63.81</b>	<b>73.11</b>	<b>78.23</b>	<b>80.92</b>	<b>77.6</b>
C10	ResNet32	ReLU	<b>88.55</b>	74.48	63.33	71.92	76.94	80.33	77.11
C10	ResNet32	SiLU	87.27	75.3	64.78	72.92	78.55	80.3	77.32
C10	ResNet32	LA-SiLU	87.85	<b>76.39</b>	<b>67.35</b>	<b>74.22</b>	<b>78.80</b>	<b>80.99</b>	<b>78.32</b>
C10	ResNet44	ReLU	<b>88.58</b>	75.2	64.32	72.75	77.87	<b>80.67</b>	77.67
C10	ResNet44	SiLU	86.65	75.11	65.67	72.73	77.84	79.85	77.1
C10	ResNet44	LA-SiLU	86.88	<b>76.73</b>	<b>69.53</b>	<b>74.98</b>	<b>78.51</b>	80.43	<b>78.43</b>
C100	ResNet20	ReLU	61.30	44.04	31.82	44.39	47.03	48.86	45.07
C100	ResNet20	SiLU	60.45	<b>45.93</b>	<b>35.66</b>	<b>46.46</b>	48.46	49.91	<b>46.59</b>
C100	ResNet20	LA-SiLU	<b>62.30</b>	45.30	31.63	45.90	<b>48.72</b>	<b>50.65</b>	46.17
C100	ResNet32	ReLU	<b>63.21</b>	45.92	33.23	46.17	49.26	50.94	46.84
C100	ResNet32	SiLU	60.04	47.14	<b>37.37</b>	<b>48.60</b>	49.57	50.33	47.41
C100	ResNet32	LA-SiLU	60.76	<b>47.26</b>	36.63	48.51	<b>49.97</b>	<b>51.03</b>	<b>47.51</b>
C100	ResNet44	ReLU	<b>64.18</b>	46.63	33.92	46.89	<b>49.68</b>	<b>51.72</b>	<b>47.75</b>
C100	ResNet44	SiLU	59.58	<b>47.41</b>	<b>38.28</b>	48.69	49.45	50.61	47.73
C100	ResNet44	LA-SiLU	60.17	47.31	38.10	<b>48.82</b>	49.63	50.26	47.46

ResNet20 and ResNet44 with SiLU demonstrated similar or greater robustness than those with LA-SiLU. This suggests that the robustness benefits of LayerAct are diminished when utilized with LN. However, it is important to note that the benefits of LayerAct may still be partially preserved even when LN is applied. For clean and noisy CIFAR10, the results were similar with those in Table 5, the networks with LA-SiLU demonstrated more robust inference compared to those with other activation functions on noisy datasets, while the performance of the deeper networks (ResNet32 and ResNet44) with ReLU were better on clean datasets than those with LA-SiLU. Furthermore, on clean datasets, the networks with LA-SiLU outperformed those with SiLU, which employs the same function (Logistic Sigmoid) for the activation scale with LA-SiLU. This indicates that the advantage of LA-SiLU, in addressing the trade-off, can enhance network performance.

Additionally, networks employing LayerAct functions with BN, which normalizes in a different dimension from that of LayerAct functions and remains the dominant normalization method for CNNs, perform effectively. In our experiments reported in the main manuscript, BN was employed for all networks, except for UNets, which do not utilize any normalization layer. The networks with LayerAct functions exhibited remarkable performance on both clean and noisy datasets. Consequently, despite the necessity for careful selection of the normalization method when using LayerAct functions, their robustness and improved performance when combined with BN make them an attractive choice for CNNs.

## I. LayerAct with Other Normalization Methods.

To investigate the relationship between LayerAct and various normalization methods, we conducted experiments on ResNets with Switchable Normalization (SN) (Luo et al. 2019), Instance enhancement batch normalization (IEBN) (Liang et al. 2020), and Decorrelated Batch Normalization (DBN) (Huang et al. 2018). We used the same experiment setting with those of our main manuscript. We report the average accuracy over 10 runs for the experiments.

Analysis of the experimental results revealed that LayerAct functions are not effectively compatible with normalizations that can cause a large variance in the channel means, such as SN and IEBN. This incompatibility arises because LayerAct is more sensitive to such large variance between channel means, which causes channels with smaller means to be more likely to become inactivated compared to those with larger means.

Table 7 demonstrates that utilizing LayerAct with SN is not effective. This ineffectiveness arises because SN

Table 7: Classification performance on CIFAR and CIFAR-C datasets with SN. We report the average mean accuracy in the table. C10 and C100 denotes CIFAR10 and CIFAR100, respectively.

Data	Model	Activation	CIFAR			CIFAR-C			
			Clean	Total	Noise	Blur	Digital	Weather	Extra
C10	ResNet20	ReLU	89.65	72.40	56.07	71.35	75.24	80.43	74.81
C10	ResNet20	SiLU	<b>90.60</b>	<b>74.17</b>	<b>57.70</b>	<b>72.94</b>	<b>77.57</b>	<b>82.21</b>	<b>76.33</b>
C10	ResNet20	LA-SiLU	89.56	72.43	55.9	71.05	75.47	80.87	74.73
C10	ResNet32	ReLU	90.70	73.90	58.24	72.84	76.3	81.79	76.42
C10	ResNet32	SiLU	<b>90.79</b>	<b>74.65</b>	<b>58.78</b>	<b>73.39</b>	<b>77.64</b>	<b>82.57</b>	<b>76.91</b>
C10	ResNet32	LA-SiLU	89.94	72.72	56.15	71.07	75.52	81.48	75.23
C10	ResNet44	ReLU	<b>91.40</b>	<b>74.65</b>	<b>58.10</b>	<b>74.01</b>	<b>77.18</b>	<b>82.81</b>	<b>76.99</b>
C10	ResNet44	SiLU	74.48	61.70	49.50	60.58	64.11	67.87	63.41
C10	ResNet44	LA-SiLU	89.36	72.02	54.85	70.59	75.07	81.05	74.24
C100	ResNet20	ReLU	57.36	37.01	20.61	38.43	39.75	43.56	38.59
C100	ResNet20	SiLU	<b>64.55</b>	<b>42.96</b>	<b>25.13</b>	<b>43.91</b>	<b>46.35</b>	<b>50.42</b>	<b>44.55</b>
C100	ResNet20	LA-SiLU	63.88	41.76	23.23	42.83	45.28	49.43	43.4
C100	ResNet32	ReLU	60.19	38.81	21.89	40.02	41.30	46.00	40.61
C100	ResNet32	SiLU	<b>64.35</b>	<b>42.45</b>	<b>25.00</b>	43.08	<b>45.86</b>	49.92	<b>44.00</b>
C100	ResNet32	LA-SiLU	64.05	42.27	23.72	<b>43.46</b>	45.50	<b>50.16</b>	43.89
C100	ResNet44	ReLU	61.64	39.93	22.64	41.03	42.47	47.54	41.67
C100	ResNet44	SiLU	44.8	29.57	18.11	29.96	31.98	34.21	30.73
C100	ResNet44	LA-SiLU	<b>62.99</b>	<b>41.91</b>	<b>22.86</b>	<b>43.06</b>	<b>46.02</b>	<b>49.79</b>	<b>43.06</b>

is a combination of BN, LN, and Instance normalization (IN) (Ulyanov, Vedaldi, and Lempitsky 2017), while the benefit of LayerAct functions diminish when preceded by LN. Additionally, LayerAct functions are more sensitive to the presence of similar channel characteristics across samples compared to element-level activation functions because the channel dimension is incorporated into normalizing dimension of LayerAct’s activation scale input. IN aggressively normalizes the mean and variance across channels towards uniformity. Therefore, given the composite normalization strategy of SN, we expect that the effect of IN will lead to a homogenization of channel characteristics, thus undermining the efficiency of LayerAct functions.

Table 8 demonstrates the performance of networks with IEBN. With the exception of ResNet20 on CIFAR100, networks with LA-SiLU demonstrated enhanced performance on noisy datasets when compared to their counterparts utilizing ReLU and SiLU. Conversely, ReLU outperformed LA-SiLU in ResNet32 and ResNet44 models. Nonetheless, it is important to highlight that LA-SiLU consistently surpassed SiLU, which utilizes the same activation scale function, across all tested scenarios. These results imply that the mechanism of LayerAct holds promise for enhancing efficiency. It is also important to consider careful consideration and integration of network complexity, particularly due to the interplay between normalization and activation functions, are essential, given that the scale function of ReLU is considerably simpler compared to sigmoid, the scale function of LA-SiLU and SiLU.

Table 9 demonstrates the performance of networks with DBN. Except for ResNet20 on CIFAR100, networks with LA-SiLU showed similar or improved performance on clean datasets, and outstanding performance on noisy datasets compared to those employing ReLU and SiLU. The results of these experiments highlight the potential applicability of LayerAct functions in conjunction with advanced batch-direction normalization methods.

## J. Additional Tables

Table 10 shows the classification performance of networks on clean CIFAR10 and CIFAR100 datasets. LA-SiLU outperformed element-level activation functions in four out of six cases. Specifically, LA-SiLU always demonstrated superior performance compared to SiLU.

Table 11 illustrates the classification performance of ResNet32 and ResNet44 on CIFAR10-C and CIFAR100-C datasets. We do not report the results for ResNet44 with PReLU on CIFAR10 due to network instability during

Table 8: Classification performance on CIFAR and CIFAR-C datasets with IEBN. We report the average mean accuracy in the table. C10 and C100 denotes CIFAR10 and CIFAR100, respectively.

Data	Model	Activation	CIFAR			CIFAR-C			
			Clean	Total	Noise	Blur	Digital	Weather	Extra
C10	ResNet20	ReLU	91.50	70.12	52.49	66.73	73.44	79.64	73.89
C10	ResNet20	SiLU	91.44	68.98	49.39	66.26	72.29	79.00	73.06
C10	ResNet20	LA-SiLU	<b>91.63</b>	<b>70.64</b>	<b>52.70</b>	<b>67.30</b>	<b>74.20</b>	<b>79.87</b>	<b>74.65</b>
C10	ResNet32	ReLU	<b>92.54</b>	71.67	54.06	<b>68.82</b>	74.82	81.12	75.11
C10	ResNet32	SiLU	91.85	71.07	53.39	68.26	73.90	80.50	74.90
C10	ResNet32	LA-SiLU	92.36	<b>71.77</b>	<b>54.19</b>	68.19	<b>75.32</b>	<b>81.15</b>	<b>75.60</b>
C10	ResNet44	ReLU	<b>92.78</b>	72.18	55.20	68.83	75.61	81.59	75.43
C10	ResNet44	SiLU	92.08	71.23	52.79	68.54	74.27	80.95	74.99
C10	ResNet44	LA-SiLU	92.50	<b>73.01</b>	<b>56.97</b>	<b>69.18</b>	<b>76.03</b>	<b>82.34</b>	<b>76.5</b>
C100	ResNet20	ReLU	66.62	<b>41.97</b>	<b>22.81</b>	<b>42.51</b>	45.07	50.30	44.37
C100	ResNet20	SiLU	66.19	40.88	21.14	41.08	44.29	49.68	43.28
C100	ResNet20	LA-SiLU	<b>66.73</b>	41.59	21.31	41.98	<b>45.26</b>	<b>50.53</b>	<b>43.82</b>
C100	ResNet32	ReLU	<b>68.17</b>	43.49	23.81	<b>43.89</b>	46.76	52.30	<b>45.78</b>
C100	ResNet32	SiLU	67.43	42.30	23.15	42.38	45.33	51.14	44.68
C100	ResNet32	LA-SiLU	67.97	<b>43.56</b>	<b>24.49</b>	43.39	<b>46.94</b>	<b>52.47</b>	45.76
C100	ResNet44	ReLU	<b>69.47</b>	44.73	25.74	44.77	47.77	53.51	47.12
C100	ResNet44	SiLU	68.18	43.47	24.76	43.37	46.46	52.22	45.89
C100	ResNet44	LA-SiLU	68.41	<b>45.29</b>	<b>26.89</b>	<b>45.15</b>	<b>48.67</b>	<b>54.03</b>	<b>47.13</b>

training. LayerAct functions outperformed the element-level activation functions in all but one instance, specifically ResNet44 on CIFAR10-C. However, it is noteworthy that LA-SiLU and LA-HardSiLU demonstrated much robust inference compared to their corresponding element-level activation functions, SiLU and HardSiLU, in all cases. Tables 12, 13, 14, 15, 16, and 17 demonstrate the standard deviation of the networks on the CIFAR and CIFAR-C dataset.

Tables 18 and 19 present the results of a statistical significance test between the accuracy of networks with element-level activation functions and those with LA-SiLU functions on clean CIFAR10 and CIFAR100. Tables 20 and 21 present the corresponding results of networks with LA-SiLU and LA-HardSiLU on CIFAR10-C and CIFAR100-C. RN20, RN32, and RN44 denotes ResNet20, ResNet32, and ResNet44. We do not report the experiments of ResNet44 with PReLU on CIFAR10 and CIFAR10-C as a network exploded during training. When the accuracies of both functions were normally distributed, we performed a T-test. In cases where at least one of them are not, we performed a Wilcoxon signed-rank test otherwise. The notation '> 0.05' indicates that the  $p$ -value from either a T-test or a Wilcoxon signed-rank test is larger than the standard significance level of 0.05 (i.e.  $p$ -value > 0.05).

Table 9: Classification performance on CIFAR and CIFAR-C with DBN. We report the average mean accuracy in the table. C10 and C100 denotes CIFAR10 and CIFAR100, respectively.

Data	Model	Activation	CIFAR			CIFAR-C			
			Clean	Total	Noise	Blur	Digital	Weather	Extra
C10	ResNet20	ReLU	90.8	65.52	35.87	65.43	71.27	78.68	68.93
C10	ResNet20	SiLU	87.69	63.55	38.16	61.21	70.24	74.77	67.01
C10	ResNet20	LA-SiLU	<b>91.72</b>	<b>69.36</b>	<b>45.68</b>	<b>67.81</b>	<b>73.41</b>	<b>80.6</b>	<b>73.37</b>
C10	ResNet32	ReLU	91.85	68.1	37.15	68.38	<b>75.07</b>	81.04	71.1
C10	ResNet32	SiLU	92.22	68.3	40.01	67.24	73.98	81.44	71.77
C10	ResNet32	LA-SiLU	<b>92.27</b>	<b>70.36</b>	<b>45.62</b>	<b>69.32</b>	74.58	<b>81.96</b>	<b>74.14</b>
C10	ResNet44	ReLU	92.35	69.79	39.25	<b>70.48</b>	76.61	<b>82.31</b>	72.67
C10	ResNet44	SiLU	<b>92.39</b>	69.48	42.19	68.97	74.63	81.63	73.13
C10	ResNet44	LA-SiLU	92.36	<b>70.17</b>	<b>44.0</b>	69.35	<b>74.63</b>	82.22	<b>74.11</b>
C100	ResNet20	ReLU	<b>58.38</b>	<b>34.19</b>	<b>13.48</b>	<b>34.26</b>	<b>38.28</b>	<b>43.67</b>	<b>36.07</b>
C100	ResNet20	SiLU	57.82	32.13	13.41	31.57	35.78	40.99	34.22
C100	ResNet20	LA-SiLU	58.19	32.24	14.32	30.95	35.11	41.4	34.96
C100	ResNet32	ReLU	54.06	30.29	14.16	28.67	34.09	38.34	32.14
C100	ResNet32	SiLU	62.0	35.26	14.99	34.41	39.35	45.01	37.46
C100	ResNet32	LA-SiLU	<b>65.02</b>	<b>38.75</b>	<b>19.18</b>	<b>37.84</b>	<b>41.81</b>	<b>48.66</b>	<b>41.36</b>
C100	ResNet44	ReLU	60.32	34.64	14.96	33.68	39.03	44.1	36.51
C100	ResNet44	SiLU	64.67	37.58	15.81	37.63	42.01	47.2	39.83
C100	ResNet44	LA-SiLU	<b>67.59</b>	<b>42.44</b>	<b>21.03</b>	<b>42.54</b>	<b>46.52</b>	<b>52.15</b>	<b>44.6</b>

]

Table 10: Classification performance on the clean CIFAR10 and CIFAR100

Activation	CIFAR10			CIFAR100		
	ResNet20	ResNet32	ResNet44	ResNet20	ResNet32	ResNet44
ReLU	91.29	92.03	92.03	65.92	67.04	68.02
LReLU	91.31	92.03	92.03	65.88	<b>67.37</b>	67.96
PReLU	90.82	92.03	-	64.00	66.35	67.68
SiLU	91.45	92.17	92.18	65.89	67.22	67.71
HardSiLU	91.09	91.77	91.42	65.19	66.49	66.38
Mish	91.48	<b>92.21</b>	92.30	65.85	67.18	68.06
GELU	<b>91.50</b>	<b>92.25</b>	<b>92.22</b>	65.84	67.30	<b>68.19</b>
ELU	91.04	91.61	91.68	<b>66.24</b>	67.01	67.55
LA-SiLU	<b>91.60</b>	92.20	<b>92.36</b>	<b>66.39</b>	<b>67.74</b>	<b>68.07</b>
LA-HardSiLU	91.21	91.68	91.36	66.16	66.63	65.51

1

Table 11: Classification performance of ResNet32 and ResNet44 on noisy CIFAR10 and CIFAR100. We report the average mean accuracy over 30 runs.

Data	Model	Activation	Total	Noise	Blur	Digital	Weather	Extra
CIFAR10-C	ResNet32	ReLU	72.00	53.07	67.62	74.75	80.44	74.41
CIFAR10-C	ResNet32	LReLU	72.01	52.66	<b>67.86</b>	<b>74.77</b>	80.42	74.5
CIFAR10-C	ResNet32	PReLU	71.7	52.82	67.06	74.72	79.90	74.17
CIFAR10-C	ResNet32	SiLU	71.7	52.37	67.21	74.08	80.51	74.38
CIFAR10-C	ResNet32	HardSiLU	71.32	52.75	66.75	73.39	79.66	74.28
CIFAR10-C	ResNet32	Mish	71.96	53.09	67.42	74.3	80.57	74.64
CIFAR10-C	ResNet32	GELU	71.64	52.44	67.18	74.11	80.26	74.26
CIFAR10-C	ResNet32	LA-SiLU	<b>72.8</b>	<b>54.02</b>	<b>68.42</b>	<b>75.13</b>	<b>81.36</b>	<b>75.51</b>
CIFAR10-C	ResNet32	LA-HardSiLU	<b>72.6</b>	<b>55.36</b>	67.71	74.70	<b>80.53</b>	<b>75.62</b>
CIFAR10-C	ResNet44	ReLU	<b>73.71</b>	<b>56.39</b>	<b>70.03</b>	<b>76.05</b>	81.27	75.92
CIFAR10-C	ResNet44	LReLU	<b>73.69</b>	56.03	<b>70.10</b>	<b>76.09</b>	<b>81.43</b>	75.81
CIFAR10-C	ResNet44	SiLU	72.45	53.12	68.64	74.80	80.88	75.06
CIFAR10-C	ResNet44	HardSiLU	72.63	55.51	68.72	74.73	79.86	75.34
CIFAR10-C	ResNet44	Mish	72.79	53.74	68.86	75.22	81.18	75.3
CIFAR10-C	ResNet44	GELU	72.82	54.65	68.69	75.26	80.85	75.24
CIFAR10-C	ResNet44	LA-SiLU	73.5	55.29	69.14	75.73	<b>81.91</b>	<b>76.19</b>
CIFAR10-C	ResNet44	LA-HardSiLU	73.33	<b>57.45</b>	68.48	75.30	80.64	<b>76.30</b>
CIFAR100-C	ResNet32	ReLU	43.51	24.10	41.99	45.81	50.58	44.32
CIFAR100-C	ResNet32	LReLU	43.58	23.8	42.12	45.94	50.73	44.42
CIFAR100-C	ResNet32	PReLU	42.44	23.72	40.31	44.81	49.42	43.27
CIFAR100-C	ResNet32	SiLU	42.94	23.06	41.27	45.01	50.31	44.02
CIFAR100-C	ResNet32	HardSiLU	42.67	23.64	40.87	44.87	49.54	43.71
CIFAR100-C	ResNet32	Mish	42.95	22.69	41.53	45.05	50.37	43.97
CIFAR100-C	ResNet32	GELU	43.00	23.15	41.45	45.21	50.21	43.94
CIFAR100-C	ResNet32	LA-SiLU	<b>44.6</b>	<b>24.16</b>	<b>43.58</b>	<b>46.74</b>	<b>52.11</b>	<b>45.51</b>
CIFAR100-C	ResNet32	LA-HardSiLU	<b>44.86</b>	<b>25.98</b>	<b>43.83</b>	<b>47.02</b>	<b>51.50</b>	<b>45.81</b>
CIFAR100-C	ResNet44	ReLU	44.77	25.45	43.05	47.33	51.94	45.44
CIFAR100-C	ResNet44	LReLU	44.8	25.57	43.26	47.17	51.91	45.5
CIFAR100-C	ResNet44	PReLU	44.31	25.78	42.19	46.7	51.44	44.97
CIFAR100-C	ResNet44	SiLU	44.04	24.52	42.61	46.16	51.08	45.01
CIFAR100-C	ResNet44	HardSiLU	44.11	26.22	42.77	46.29	50.32	44.9
CIFAR100-C	ResNet44	Mish	44.14	24.18	42.69	46.36	51.37	45.11
CIFAR100-C	ResNet44	GELU	43.93	24.39	42.29	46.15	51.02	44.85
CIFAR100-C	ResNet44	LA-SiLU	<b>46.12</b>	<b>26.68</b>	<b>44.94</b>	<b>48.32</b>	<b>53.44</b>	<b>46.89</b>
CIFAR100-C	ResNet44	LA-HardSiLU	<b>46.83</b>	<b>30.85</b>	<b>45.83</b>	<b>48.93</b>	<b>52.5</b>	<b>47.35</b>

Table 12: Standard deviation of ResNet20s’ accuracy on CIFAR10 and CIFAR10-C with different activation functions. We average in the table.

Activation	Clean	Total	Noise	Blur	Digital	Weather	Extra
ReLU	0.2120	1.3171	2.4428	1.5145	0.9736	0.7231	1.2127
LReLU	0.2635	1.2630	2.2750	1.4947	0.8948	0.6938	1.2099
PReLU	0.2323	1.4176	2.4859	1.4106	1.3038	0.8178	1.3369
SiLU	0.2057	1.1067	1.7695	1.3471	0.8738	0.7012	1.0076
HardSiLU	0.2287	1.2052	2.3675	1.4039	0.8074	0.6465	1.0914
MISH	0.2302	1.1507	2.1373	1.3116	0.7921	0.6335	1.1255
GELU	0.1868	1.1358	1.8216	1.5201	0.8537	0.5251	1.1298
ELU	0.1742	1.1673	2.2787	1.3572	0.7776	0.5961	1.1047
LA-SiLU	0.1645	1.1800	1.8781	1.4681	0.9738	0.7475	1.0069
LA-HardSiLU	0.2051	1.1765	2.3889	1.1128	0.9142	0.7081	1.0616

Table 13: Standard deviation of ResNet32s’ accuracy on CIFAR10 and CIFAR10-C with different activation functions. We average in the table.

Activation	Clean	Total	Noise	Blur	Digital	Weather	Extra
ReLU	0.3880	1.5955	2.8978	1.7971	1.3270	0.9254	1.3556
LReLU	0.3356	1.7599	3.0043	2.1394	1.4202	1.0200	1.5270
PReLU	0.2809	1.6875	2.6927	1.8571	1.6496	0.9261	1.5634
SiLU	0.2188	1.3848	2.7176	1.7485	0.8207	0.7220	1.2483
HardSiLU	0.2200	1.2341	2.0973	1.5508	0.8625	0.8104	1.0653
MISH	0.2497	1.2869	2.1864	1.7262	0.8797	0.6475	1.2194
GELU	0.1568	1.2598	2.3925	1.4798	0.8745	0.6164	1.2188
ELU	0.1800	1.2041	1.8703	1.5525	0.9373	0.7095	1.1177
LA-SiLU	0.1898	1.2232	1.9876	1.4006	1.1328	0.6804	1.1056
LA-HardSiLU	0.3023	1.4008	2.2405	1.7160	1.1416	0.8028	1.3129

Table 14: Standard deviation of ResNet44s’ accuracy on CIFAR10 and CIFAR10-C with different activation functions. We average in the table.

Activation	Clean	Total	Noise	Blur	Digital	Weather	Extra
ReLU	0.6249	2.1269	3.5833	2.4709	1.8301	1.2399	1.8742
LReLU	0.4437	1.9929	3.3751	2.3684	1.6750	1.1650	1.7264
PReLU	14.5207	11.3037	8.8671	10.8069	11.8174	12.5987	11.8192
SiLU	0.2435	1.4765	2.6747	1.7969	1.0507	0.8144	1.3453
HardSiLU	0.4192	1.7214	3.2993	1.8791	1.3047	1.0844	1.4341
MISH	0.4472	2.1393	3.7470	2.5737	1.6741	1.2354	1.8683
GELU	0.4696	1.6769	3.1032	1.8889	1.2754	0.8846	1.5892
ELU	0.2073	1.4907	2.7899	1.7389	1.1132	0.7598	1.3765
LA-SiLU	0.2719	1.3634	2.5109	1.5678	1.0625	0.7445	1.2180
LA-HardSiLU	0.2033	1.5738	2.8731	1.7762	1.3225	0.8906	1.3316

Table 15: Standard deviation of ResNet20s’ accuracy on CIFAR100 and CIFAR100-C with different activation functions. We average in the table.

Activation	Clean	Total	Noise	Blur	Digital	Weather	Extra
ReLU	0.2937	0.8120	1.0754	0.9131	0.7956	0.5861	0.7558
LReLU	0.3233	0.8633	1.0476	0.8994	0.7943	0.7862	0.8353
PReLU	0.4435	0.9101	1.2044	1.0421	0.8121	0.7970	0.7682
SiLU	0.4147	0.7665	1.0922	0.8286	0.6642	0.5197	0.8095
HardSiLU	0.3903	0.8104	1.1921	0.8172	0.6649	0.6375	0.8356
MISH	0.3269	0.7400	1.0435	0.6064	0.7377	0.6462	0.7420
GELU	0.3866	0.8059	0.9036	0.9290	0.8281	0.6220	0.7714
ELU	0.3618	0.7367	1.0898	0.7222	0.6868	0.5689	0.7044
LA-SiLU	0.3493	0.8537	1.3183	0.8409	0.7137	0.6806	0.8313
LA-HardSiLU	0.4056	0.8751	1.2555	0.8963	0.7188	0.7466	0.8536

Table 16: Standard deviation of ResNet32s’ accuracy on CIFAR100 and CIFAR100-C with different activation functions. We average in the table.

Activation	Clean	Total	Noise	Blur	Digital	Weather	Extra
ReLU	0.5187	1.0671	1.3930	1.1459	1.0240	0.8663	0.9876
LReLU	0.3364	0.9092	1.3616	0.8028	0.9881	0.6881	0.8184
PReLU	0.5045	0.9674	1.2581	1.0727	0.8316	0.8351	0.9123
SiLU	0.5053	1.0087	1.5275	1.0608	0.8957	0.6965	0.9926
HardSiLU	0.5325	0.9114	0.9530	1.0173	0.9229	0.9203	0.7538
MISH	0.4820	0.9148	1.2750	0.9058	0.8194	0.7269	0.9369
GELU	0.4418	0.8121	1.0506	0.9158	0.7070	0.6675	0.7790
ELU	1.4877	1.3180	1.1907	1.3131	1.3876	1.4028	1.2640
LA-SiLU	0.3776	0.8765	1.3721	0.8750	0.6403	0.6864	0.9326
LA-HardSiLU	0.4486	0.9763	1.5039	1.0204	0.8062	0.7838	0.8988

Table 17: Standard deviation of ResNet44s’ accuracy on CIFAR100 and CIFAR100-C with different activation functions. We average in the table.

Activation	Clean	Total	Noise	Blur	Digital	Weather	Extra
ReLU	0.5652	1.1011	1.5926	1.1677	0.9634	0.9098	0.9947
LReLU	0.6872	1.2173	1.8513	1.1183	1.1814	0.9895	1.1046
PReLU	0.7084	1.3226	1.8320	1.4481	1.0939	1.2049	1.1616
SiLU	0.5204	0.9563	1.2746	0.9791	0.8475	0.8444	0.9157
HardSiLU	0.9417	1.4808	1.6740	1.5590	1.5011	1.3818	1.3362
MISH	0.5119	0.9386	1.3795	0.9206	0.7863	0.7879	0.9291
GELU	0.6182	0.9809	1.3545	0.9600	0.9044	0.8583	0.9207
ELU	0.4118	1.1195	1.6396	1.1471	0.9781	0.8948	1.0679
LA-SiLU	0.4366	1.1648	1.5511	1.2528	1.1577	0.9353	1.0238
LA-HardSiLU	0.7955	1.8629	2.9063	1.8458	1.6924	1.5680	1.5630

Table 18: Statistical significance test of LA-SiLU on CIFAR10 dataset.

	LA-SiLU							
	ReLU	LReLU	PReLU	SiLU	HardSiLU	Mish	GELU	ELU
RN20	$< 1e^{-3}$	$< 1e^{-3}$	$< 1e^{-3}$	0.002	$< 1e^{-3}$	0.011	0.016	$< 1e^{-3}$
RN32	0.02	0.011	0.005	0.331	$< 1e^{-3}$	0.422	0.125	$< 1e^{-3}$
RN44	0.014	0.001	-	0.007	$< 1e^{-3}$	0.479	0.094	$< 1e^{-3}$



## K. Additional Figures

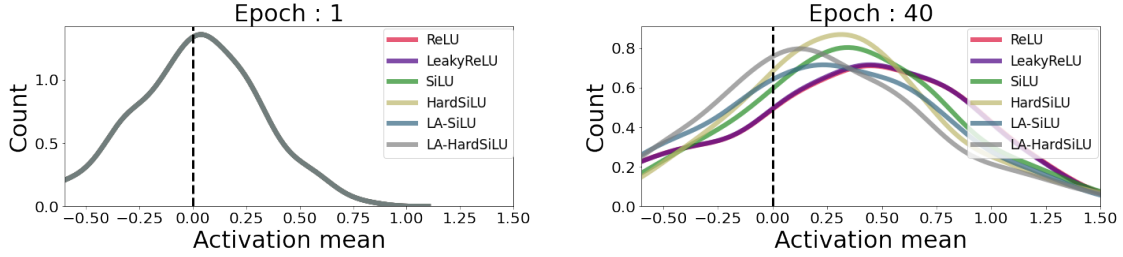


Figure 8: Distribution of the activation **input** means of the elements in a trained network on MNIST at 1<sup>st</sup> and 40<sup>th</sup> epochs.

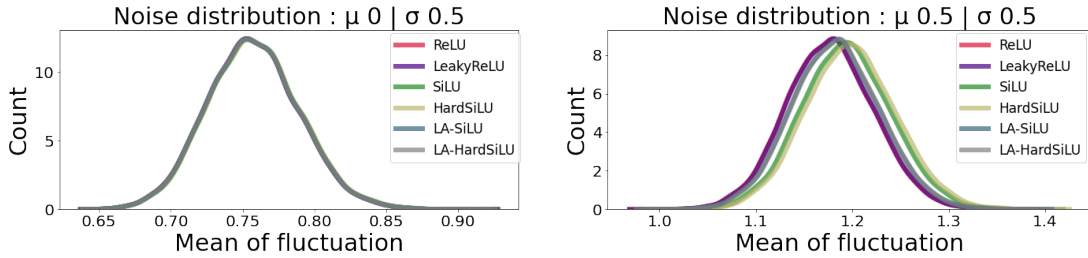


Figure 9: Distribution of activation **input** fluctuation due to noise with different noise distribution.

In this section, we present additional tables and figures extracted from the experiments. Figure 8 presents the distribution of the mean activation input. As observed in the mean of activation input at epoch 40 (right), LayerAct functions promote the training of parameter  $W$  such that the output of the linear projection  $y = W^T x$ , which is also activation input, gets closer to zero compared to other functions. This helps the activation output to exhibit a ‘zero-like’ behaviour.

LayerAct functions exhibit a significantly lower mean and variance of activation fluctuation among the samples compared to any other element-level activation function (see Figure 3 in the main manuscript). Figure 9 demonstrates that the distribution of mean fluctuation in activation input appears similar across all functions. This observation confirms that the lower mean and variance of activation output fluctuation of LayerAct functions is not due to a smaller fluctuation in activation input, but is a result of the inherent mechanism of LayerAct.

## L. Medical Image

In this section, we present the setting of experimental result from U-net (Olaf Ronneberger 2015) and Unet++ (Zhou et al. 2018) for segmentation task on a nuclei image dataset from Data Science Bowl 2018 (Goodman et al. 2018). Detailed experimental setting is as follows: (1) Adam optimizer with  $3e^{-4}$  learning rate, and  $1e^{-4}$  weight decay, (2) training 100 epoches with cosine annealing scheduler, and (3) BCE-Dice Loss as the loss function. We report the average IoU (Intersection over Union; %) over 10 trials with different weight initialization in Table 4 of the main manuscript.

## M. Adversarial Robustness

We conducted experiments to investigate the adversarial robustness of LayerAct. We utilized ReLU, SiLU, and LA-SiLU as the activation of ResNet18. The experimental setting was based on (Zhou et al. 2023). The experimental results in Table 4 in the main manuscript show that the ResNet20 with LA-SiLU is more robust

against adversarial attacks compared to those with other activations. These results indicate that LayerAct can enhance adversarial robustness as well.

---

# Layer-level activation mechanism

---

**Kihyuk Yoon**

Department of Industrial Engineering  
UNIST

**Chiehyeon Lim**

Department of Industrial Engineering  
UNIST

## Abstract

In this work, we propose a novel activation mechanism aimed at establishing layer-level activation (LayerAct) functions. These functions are designed to be more noise-robust compared to traditional element-level activation functions by reducing the layer-level fluctuation of the activation outputs due to shift in inputs. Moreover, the LayerAct functions achieve a zero-like mean activation output without restricting the activation output space. We present an analysis and experiments demonstrating that LayerAct functions exhibit superior noise-robustness compared to element-level activation functions, and empirically show that these functions have a zero-like mean activation. Experimental results on three benchmark image classification tasks show that LayerAct functions excel in handling noisy image datasets, outperforming element-level activation functions, while the performance on clean datasets is also superior in most cases.

## 1 Introduction

Various activation functions have been proposed to enhance the effectiveness and efficiency of neural networks training. Previous studies have identified significant properties of activation functions: i) one-sided saturation (e.g., rectified linear unit (ReLU [7, 20]) that saturates only negative side of outputs) to avoid the vanishing gradient problem while maintaining noise-robustness, and ii) allowing negative output for a zero-like mean of activation (see Appendix A for mathematical definition of zero-like mean activation) for effective and efficient training [4, 22]. Modern activation functions, such as exponential linear unit (ELU [4]), flexible ReLU (FReLU, [4, 22]), and sigmoid-weighted linear unit (SiLU, also known as Swish, [5, 23]), seek a balance between the properties. They only saturate the large negative outputs for noise-robustness, while allowing the activation functions to produce small negative outputs for zero-like mean activation.

Nevertheless, existing activation functions that operate on a single element of the activation input (i.e., a unit of a layer) exhibit two limitations underlying their element-level activation mechanisms. Firstly, there is a trade-off between two properties of element-level activation, one-sided saturation (limiting negative output space) and allowing negative outputs. One-sided saturation naturally restricts the negative space of the activation outputs, leading the mean of activation outputs to be far from zero. This trade-off is apparent not only in ReLU, which never permits negative outputs, but also in the activation functions like ELU or FReLU that allow small negative outputs. Secondly, the noise-robustness varies across samples. The noise-robustness of element-level activation functions relies only on saturation state. This implies that existing activation functions can ensure noise-robustness for samples only when a sufficiently large number of elements are in the saturation state, not when there are fewer elements in the saturation state.

To address these issues with element-level activation functions, we propose a novel activation mechanism and two LayerAct functions, denoted as LA-SiLU and LA-HardSiLU. The trade-off problem of element-level activation functions arises because the activation input space that leads activation outputs to be in saturation state remains fixed across all samples. Unlike the element-level activation mechanism, our proposed layer-level activation mechanism assigns the saturation state

based on the normalized input of the layer-dimension, similar to layer normalization (LayerNorm; [1]). As a result, the activation output space of the saturation state varies between samples; the activation input space leading to saturation state is determined by the layer-dimension mean and variance. Furthermore, the noise-robustness of LayerAct functions does not fully depend on the number of the elements in the saturation state. We demonstrate that the upper bound of activation fluctuation due to shift of layer input can be lower with LayerAct functions than with element-level activation functions.

Experimental analysis with the MNIST image dataset revealed the following properties of the LayerAct functions: i) the mean activation of LayerAct functions is zero-like, and ii) the output fluctuation due to noisy input is smaller with these functions than that with element-level activation functions. Additionally, we compared the performance of the LayerAct functions with other element-level activation functions on three image classification tasks. The results on noisy CIFAR10 and CIFAR100 datasets demonstrate that LayerAct functions were superior to other element-level activation functions. Furthermore, ResNet50 with LayerAct functions also showed superior performance on both clean and noisy ImageNet datasets compared to other functions.

## 2 Background

### 2.1 Activation scale

Consider a layer in a multi-layer perceptron with linear projection and an activation function. The computation of this layer, given a  $r$ -dimensional input vector  $x = (x_1, x_2, \dots, x_r)^T$ , a weight matrix  $W \in \mathbb{R}^{r \times d}$ , and non-linear activation function  $f$  is defined as follows:

$$y = W^T x, \quad a = f(y), \quad (1)$$

where  $y = (y_1, y_2, \dots, y_d)^T$  and  $a$  are the  $d$ -dimensional output vectors of the linear projection and activation of a layer, respectively. The output vector  $y$  of the linear projection and activation vector  $a$  serves as the input of the activation function and the input of the next layer, respectively.

In some activation functions, a function bounded between one and zero characterizes the non-linearity of the activation function during forward-propagation. We define this function, denoted as  $s$ , and its output as the *activation scale function* and *activation scale*, respectively. The activation output during forward pass and gradient during backward pass of an element-level activation functions with activation scale function  $s$  are:

$$a_i = y_i s(y_i), \quad \frac{\partial a_i}{\partial y_i} = s(y_i) + y_i \frac{\partial s(y_i)}{\partial y_i}, \quad (2)$$

where  $s$  is increasing and  $s(y_i) > 0$  if  $y_i > 0$ . For example, the activation scale functions for the  $i^{\text{th}}$  element in ReLU and SiLU, are presented as follows:

$$s^{\text{ReLU}}(y_i) = \begin{cases} 1, & \text{if } y_i \geq 0 \\ 0, & \text{if } y_i < 0 \end{cases}, \quad s^{\text{SiLU}}(y_i) = \frac{1}{1 + e^{-y_i}} \quad (3)$$

where  $y_i$ , *sigmoid*,  $s^{\text{ReLU}}$ , and  $s^{\text{SiLU}}$ , present the  $i^{\text{th}}$  element of  $y$ , Logistic Sigmoid function, and the non-linear scale functions of ReLU and SiLU, respectively.

Furthermore, the saturation state of such activation functions can be defined using the activation scale:

**Definition 2.1** (Saturation state of activation functions with activation scale functions). *The saturation state of an activation function with an activation scale function  $s$  is when  $s(y_i) \simeq 0$ , as the activation output  $a_i = y_i s(y_i)$  reaches saturation.*

In conclusion, the activation scale function plays a crucial role in providing non-linearity during the forward pass, controlling the gradient during the backward pass, and determining the saturation state of the activation function.

### 2.2 Trade-off between saturation and zero-like mean activation

Element-level activation functions that exhibit saturation, such as ReLU, are well recognized for their noise-robustness properties, for instance, samples with a large number of elements in the saturation

state are noise-robust [4, 22]). However, the saturation in these functions does not allow negative outputs, which causes the mean of the activation outputs to be far from zero, potentially leading to inefficient training [4].

To address this issue, recent activation functions, such as ELU, FReLU, and SiLU, saturate only the large negative outputs. These activation functions can achieve a zero-like mean activation with small negative outputs. However, a trade-off still exists because the restriction of negative outputs, designed to ensure saturation, prevents the allowance of large negative outputs, thereby restraining the mean of activation from being more zero-like. Additionally, saturation that relies solely on the input of a single element can result a large variance in noise-robustness between samples.

### 2.3 Large variance of noise-robustness across samples

To analyze the noise-robustness, we define activation fluctuation (i.e., fluctuation of activation outputs due to the shift of inputs) that can represent the layer-level noise-robustness on a sample.

**Definition 2.2** (Activation fluctuation). *Let  $\epsilon = (\epsilon_1, \epsilon_2, \dots, \epsilon_d)^T$  be the noise vector. We define activation fluctuation as  $\|f(y + \epsilon) - f(y)\| \leq c$ , where  $c$  is the upper bound of activation fluctuation.*

The lower the upper bound  $c$  is, the lower the variance of noise-robustness across samples. We can define the activation fluctuation of element-level activation functions:

**Definition 2.3** (Activation fluctuation of element-level activation functions). *Let  $\epsilon_i$  be the  $i^{\text{th}}$  noise, and  $\hat{y}_i = y_i + \epsilon_i$ . The activation fluctuation of element-level activation function  $f$  is given by:*

$$\|f(\hat{y}) - f(y)\| = \sum_{i=1}^d |\hat{y}_i s(\hat{y}_i) - y_i s(y_i)| = \sum_{i=1}^d |y_i (s(\hat{y}_i) - s(y_i)) + \epsilon_i s(\hat{y}_i)|,$$

A sample will exhibit a small  $\|f(\hat{y}) - f(y)\|$  if a sufficient number of its elements are in saturation state. However, element-level activation functions do not ensure that all samples have a sufficient number of elements in saturation state. More specifically, the activation fluctuation is upper-bounded when not all elements are in the saturation state, where  $y_i > 0$  for all  $i$ :

$$\|f(\hat{y}) - f(y)\| \leq \sum_{i=1}^d (y_i |s(\hat{y}_i) - s(y_i)| + |\epsilon_i| \cdot s(\hat{y}_i)) \quad (4)$$

Equation 4 demonstrates that activation scale is closely related to the activation fluctuation, samples with large  $\|s(\hat{y}) - s(y)\|$  and  $\|s(\hat{y})\|$  are not robust to noise. Thus, a method that can reduce the upper bound of  $\|s(\hat{*}) - s(*)\|$  and  $\|s(\hat{*})\|$  will reduce the upper bound of activation fluctuation, resulting in a low variance of noise-robustness across samples.

### 2.4 Layer Normalization

LayerNorm normalizes elements along the layer-dimension, as opposed to the batch-dimension in batch normalization (BatchNorm, [11]). LayerNorm normalizes the elements of a layer using the layer-dimension mean  $\mu_y$  and standard deviation  $\sigma_y$  defined as follows:

$$n_i^{LN} = \frac{g_i}{\sigma_y} (y_i - \mu_y) + b_i, \quad \mu_y = \frac{1}{d} \sum_{i=1}^d y_i, \quad \sigma_y = \sqrt{\frac{1}{d} \sum_{i=1}^d (y_i - \mu_y)^2} \quad (5)$$

where  $n_i^{LN}$ ,  $g_i$ , and  $b_i$  are the  $i^{\text{th}}$  normalized output, gain, and bias of LayerNorm. With LayerNorm, the sum of activation scale  $\|s(n^{LN})\|$  will be similar across all samples, which helps to reduce the variance of noise-robustness across all samples. However, LayerNorm loses all the mean and variance statistics of linear projection  $y$ ; thus, the final outputs of the layer across samples become similar [14, 17]. To avoid this dilution problem, a layer-level balancing mechanism should be employed that does not directly re-scale or re-center the activation input.

In this section, we have defined activation scale function and demonstrated its critical role in activation processes: 1) provides non-linearity during forward pass, 2) controls gradient during backward pass, and 3) is related to the noise-robustness of the model. We demonstrated that element-level activation functions may have large variance of noise-robustness across samples. LayerNorm can reduce such variance of the noise-robustness by re-scaling and re-centering the activation input, but it also causes the statistics of activation outputs to be similar across all samples.

### 3 Layer-level activation

In this section, we introduce and discuss a novel layer-level activation mechanism and associated functions that utilize layer-dimension normalized input for the activation scale function (see Figure 1). Our proposed method does not suffer from the trade-off issue and exhibits lower variance than element-level activation functions across samples. Importantly, it does not cause the dilution problem that statistics of activation outputs to become similar.

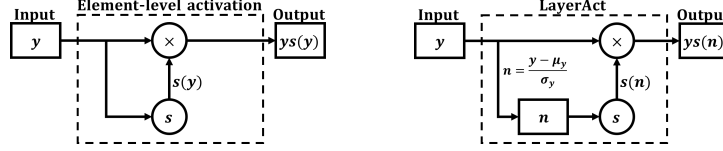


Figure 1: The mechanisms of the element-level activation (left) and proposed layer-level activation (right).

#### 3.1 LayerAct mechanism

The LayerAct function is defined as the product of the input  $y_i$  and the activation scale  $s(n_i)$  which uses the layer-normalized input  $n_i$ . The forward pass of a LayerAct function is given by:

$$a_i = y_i s(n_i), \quad n_i = \frac{(y_i - \mu_y)}{\sqrt{\sigma_y^2 + \alpha}} \quad (6)$$

where  $\alpha > 0$  is a constant that introduced for stability,  $\mu_y$ , and  $\sigma_y$  are the layer-dimension mean and standard deviation, respectively. Using the chain rule, the backward pass can be described as follows:

$$\begin{aligned} \frac{\partial \mathcal{L}}{\partial \mu} &= \sum_{i=1}^d \frac{\partial \mathcal{L}}{\partial a_i} \cdot \frac{\partial s(n_i)}{\partial n_i} \cdot \frac{-y_i}{\sqrt{\sigma^2 + \alpha}}, \\ \frac{\partial \mathcal{L}}{\partial \sigma^2} &= \sum_{i=1}^d \frac{\partial \mathcal{L}}{\partial a_i} \cdot \frac{\partial s(n_i)}{\partial n_i} \cdot \frac{-y_i \cdot n_i}{2(\sigma^2 + \alpha)}, \\ \frac{\partial \mathcal{L}}{\partial y_i} &= \frac{\partial \mathcal{L}}{\partial a_i} s(n_i) + \frac{\partial \mathcal{L}}{\partial a_i} \cdot \frac{\partial s(n_i)}{\partial n_i} \cdot \frac{y_i}{\sqrt{\sigma^2 + \alpha}} \\ &\quad + \frac{1}{d} \cdot \frac{\partial \mathcal{L}}{\partial \mu} + \frac{2(y_i - \mu)}{d} \cdot \frac{\partial \mathcal{L}}{\partial \sigma^2}. \end{aligned}$$

Notably, the activation output  $a_i$  in Equation 6 is not normalized output of activation input  $y$ . Unlike activation with LayerNorm, which results in the activation output  $a_i = n_i s(n_i)$  and erases all mean and variance statistics from the input vector, the LayerAct functions can deliver the mean and variance of input to output. For the detail on difference between LayerAct and activation with LayerNorm, see Appendix B.

For stable learning and inference, it is crucial for the activation outputs to remain continuous throughout the entire output space. While element-level activation functions such as ReLU, leaky ReLU (LReLU [18]), and parametric ReLU (PReLU, [8]) do not require the activation scale to be continuous at zero (since the activation output  $y_i s(y_i)$  is still continuous at zero), this is not the case for LayerAct functions, where the activation output  $y_i s(n_i)$  is discontinuous if the activation scale function is not continuous. Hence, we define specific activation scale function  $s$  for LayerAct mechanism:

**Definition 3.1** (Activation scale function for LayerAct functions). *The activation scale function  $s$  is an increasing Lipschitz continuous function that bounded between zero and one:*

$$s(0) = 1/2, \quad |s(a) - s(b)| \leq K |a - b| \quad \forall a, b \in \mathbb{R}.$$

Any function that satisfies Definition 3.1 can be used as an activation scale function for a LayerAct function. In this paper, we suggest the Sigmoid and HardSigmoid functions as simple activation scale functions for LayerAct functions. Both the functions are Lipschitz continuous functions and bounded between 0 and 1. We propose the following two LayerAct functions, LA-SiLU and LA-HardSiLU, which are the layer-level transformed versions of SiLU and HardSiLU, respectively:

$$LA-SiLU(y_i) = \frac{y_i}{1 + e^{-n_i}}, \quad LA-HardSiLU(y_i) = \begin{cases} y_i, & \text{if } n_i \geq 3 \\ y_i \left(\frac{n_i}{6} + \frac{1}{2}\right), & \text{if } -3 \leq n_i < 3 \\ 0, & \text{if } n_i < -3 \end{cases}.$$

### 3.2 Properties of LayerAct

**No trade-off between saturation and negative outputs.** LayerAct, unlike element-level activations, bypasses the trade-off between saturation and zero-like mean activation. The key distinction in saturation between the element-level and LayerAct functions is that saturation state of element-level functions requires to be fixed at a certain point of activation output, whereas that of LayerAct functions depends on layer-dimension normalized inputs. Thus, while LayerAct still have saturation state where  $s(n_i) \simeq 0$ , the activation output space with a LayerAct function is not limited (e.g., consider a layer where  $\mu_y \ll 0$ ).

**Relationship with normalization methods.** The LayerAct functions can be used in conjunction with normalization methods that have different normalization direction, such as BatchNorm, which have been successful across various deep learning domains [2]. Conversely, the beneficial properties of LayerAct might be diminished when it is used right after LayerNorm, where the activation inputs are already normalized in layer-direction. However, this does not imply that the LayerAct functions are unsuitable for networks with LayerNorm. LayerAct functions can be employed in networks where the activation and LayerNorm do not correspond one-to-one, such as the LSTM-based models presented by Ba et al. [1]. For the detail, see Appendix C.

### 3.3 Noise-robustness of LayerAct

In this subsection, we begin by establishing that the activation fluctuation of LayerAct is also related to the two terms of activation scale function,  $\|s(\hat{*}) - s(*)\|$  and  $\|s(\hat{*})\|$ , as outlined in Subsection 2.3. Subsequently, we demonstrate that these two terms for LayerAct are bound to be lower than those of element-level activation. Here, we consider noise that is not substantial compared to activation input (i.e.,  $\sigma_\epsilon \ll \sigma_y$ ), where  $\sigma_\epsilon$  represents the variance of noise  $\epsilon$ . To begin with, we define the activation fluctuation of LayerAct.

**Definition 3.2** (Activation fluctuation of LayerAct functions). *The activation fluctuation of LayerAct activation function  $g$ , where  $\hat{n}_i = (\hat{y}_i - \mu_{\hat{y}}) / \sigma_{\hat{y}}$  denotes  $i^{\text{th}}$  noisy normalized input, is defined as:*

$$\|g(\hat{y}) - g(y)\| = \sum_{i=1}^d |\hat{y}_i s(\hat{n}_i) - y_i s(n_i)| = \sum_{i=1}^d |y_i (s(\hat{n}_i) - s(n_i)) + \epsilon_i s(\hat{n}_i)|,$$

Given that  $n$  and  $\hat{n}$  represent the normalized output of  $y$  and  $\hat{y}$ , respectively, we can define an upper bound for the activation fluctuation of LayerAct functions as follows:

$$\|g(\hat{y}) - g(y)\| \leq \sum_{i=1}^d (|y_i| |s(\hat{n}_i) - s(n_i)| + |\epsilon_i| s(\hat{n}_i)). \quad (7)$$

Hence, the two terms of LayerAct scale function,  $\|s(\hat{n}) - s(n)\|$  and  $\|s(\hat{n})\|$ , are also related to the noise-robustness, similar to those of element-level activation function (see Equation 4). Considering Definition 3.1, the upper bound of  $\|s(\hat{y}) - s(y)\|$  and  $\|s(\hat{y})\|$  of element-level activation and that of  $\|s(\hat{n}) - s(n)\|$  and  $\|s(\hat{n})\|$  of LayerAct are given by respectively:

$$\|s(\hat{y}) - s(y)\| \leq \sum_{i=1}^d K |\epsilon_i|, \quad \|s(\hat{y}_i)\| \leq d, \quad (8)$$

$$\|s(\hat{n}) - s(n)\| < K \sum_i^d \left| \frac{y_i + \epsilon_i - \mu_y - \mu_\epsilon}{\sqrt{\sigma_y^2 + \alpha + \sigma_\epsilon^2}} - \frac{y_i - \mu_y}{\sqrt{\sigma_y^2 + \alpha}} \right| = \sum_i^d \frac{K |\epsilon_i - \mu_\epsilon|}{\sqrt{\sigma_y^2 + \alpha}}, \quad \|s(\hat{n}_i)\| = \frac{d}{2}, \quad (9)$$

where  $\sqrt{\sigma_y^2 + \alpha + \sigma_\epsilon^2} \simeq \sqrt{\sigma_y^2 + \alpha} > 1$  when  $\sigma_y \gg \sigma_\epsilon$  and  $\alpha$  is sufficiently large.

Equation 8 and 9 reveal that the activation fluctuation of LayerAct can exhibit a smaller boundary across samples compared to that of element-level activation. This suggests that LayerAct can ensure more robust processing during forward pass of a network. Moreover, the noise-robustness of the LayerAct does not fully rely on the saturation state, which can cause negative effects in training a network [26].

## 4 Experiment

In this section, we present the experimental analysis and classification performance of LayerAct. First, we verify the important properties of LayerAct with the MNIST dataset. Next, we evaluate the classification performance of the LayerAct functions on three image datasets, CIFAR10, CIFAR100 [12], and ImageNet [24] for both clean and noisy cases. We used ResNets as the network architecture for our experiments [9]. See Appendix E for details of the experimental environment, and Appendix G for more result of experiments.

### 4.1 Experimental analysis on MNIST

In this subsection, we compare the LayerAct functions with other activation functions to demonstrate that LayerAct functions embody the properties discussed in Section 3: i) zero-like mean activation and ii) noise-robustness. We trained a network with a single layer that contains 512 elements on the MNIST training dataset without any noise to observe the behavior of the LayerAct functions during training. For the detail of experimental setting, see Appendix E.

#### 4.1.1 Zero-like mean activation

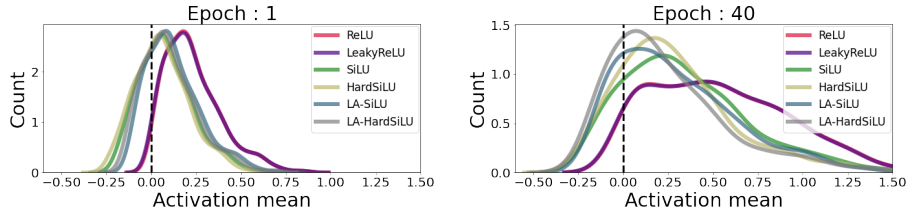


Figure 2: Distribution of the activation output means of the elements in a trained network on MNIST at 1 and 40 epochs. The distributions did not change after 40 epochs. The LayerAct functions maintain zero-like mean activation for all epochs.

Figure 2 shows the distribution of the activation output means of the single-layer network trained on the MNIST dataset. Our experimental results indicate that the LayerAct functions allow similar (before epoch 20) or larger (after epoch 40) negative outputs compared to the element-level activation functions with negative outputs. Thus, LA-SiLU and LA-HardSiLU can achieve more zero-like mean activation than other activation functions.

#### 4.1.2 Noise-robustness

To confirm the noise-robustness of the LayerAct functions, we computed the activation fluctuation of Definition 2.3 and 3.2 using the network trained on the clean MNIST dataset. For the noisy input  $\hat{y}_i$ , we used two different noises with a normal distribution.

Figure 3 shows the distribution of the activation fluctuation with two different noise distributions. Although the fluctuation distribution of the activation input was similar (See Figure 4 in Appendix G), LayerAct functions have a significantly smaller mean and variance of activation fluctuation among the samples than any other element-level activation function in all cases. The decrease in variance is remarkable, showing that the LayerAct functions are noise-robust for all samples. Moreover, the element-level activation functions that ensure a zero-like mean with one-sided saturation such as SiLU or HardSiLU showed slightly larger activation fluctuations than those of ReLU or LReLU when

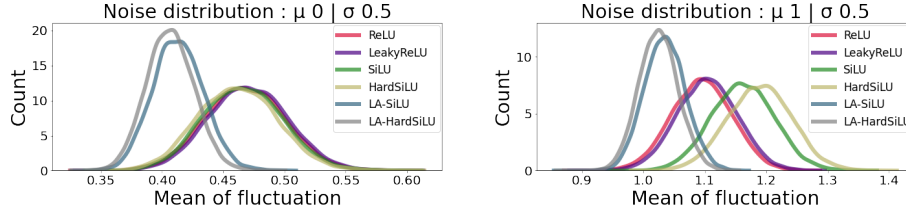


Figure 3: Distribution of activation output fluctuation due to noise with different noise distribution. The activation fluctuation of the LayerAct functions have lower mean and variance than those of the other element-level activation functions in both cases.

the noise had a large mean. However, the LayerAct functions maintained lower fluctuations in both cases.

## 4.2 Classification performance

We demonstrate the classification performance of the LayerAct functions on three image datasets, CIFAR10, CIFAR100, and ImageNet. We trained ResNet20, ResNet32, and ResNet44 with a basic block for CIFAR10 and CIFAR100. For ImageNet, we trained ResNet50 with the bottleneck block. In all our experiments, we utilized networks with BatchNorm. We compared the LayerAct functions with ReLU, LReLU, PReLU, Mish[19], SiLU and HardSiLU. We used accuracy as the performance metric. See Appendix E for the detail of experimental setting.

Table 1: Classification performance on the clean CIFAR10 and CIFAR100.

	CIFAR10			CIFAR100		
	ResNet20	ResNet32	ResNet44	ResNet20	ResNet32	ResNet44
ReLU	91.29	92.03	92.03	65.92	67.04	68.02
LReLU	91.31	92.03	92.03	65.88	<b>67.37</b>	67.96
PReLU	90.82	92.03	-	64.00	66.35	67.68
Mish	<b>91.48</b>	<u>92.21</u>	<b>92.30</b>	65.85	67.18	<b>68.06</b>
SiLU	91.45	92.17	92.18	65.89	67.22	67.71
HardSiLU	91.09	91.77	91.42	65.19	66.49	66.38
LA-SiLU	<b>91.60</b>	<b>92.20</b>	<b>92.36</b>	<b>66.39</b>	<b>67.74</b>	<b>68.07</b>
LA-HardSiLU	91.21	91.68	91.36	<b>66.16</b>	66.63	65.51

### 4.2.1 CIFAR10 and CIFAR100

Table 1 presents the average classification performance of both LayerAct functions and element-level activation functions over 30 runs, benchmarked on the clean CIFAR10 and CIFAR100 dataset. The best results are underlined and bolded, while the second best are bolded. One trial of Resnet44 with PReLU on CIFAR10 exploded during training. Among the element-level activation functions, networks with Mish outperformed other functions on CIFAR10, whereas ResNet20 with ReLU and ResNet32 with LReLU exhibited superior performance on CIFAR100. However, the performance of LA-SiLU was stable, showing similar or better performance than other activation functions in most cases. In statistical significance test, networks with LA-SiLU outperformed a significant majority, specifically 30 out of 36, of networks with element-level activation functions (T-test or Wilconxon signed-rank test with  $p$ -value < 0.05).

### 4.2.2 Noisy CIFAR10 and CIFAR100

To verify the noise-robustness of LayerAct functions, we evaluated their classification performance on the noisy datasets, using networks that were trained on clean datasets. We selected three different types of noise which are easily found in real-world datasets: Gaussian distributed noise [25], Poisson

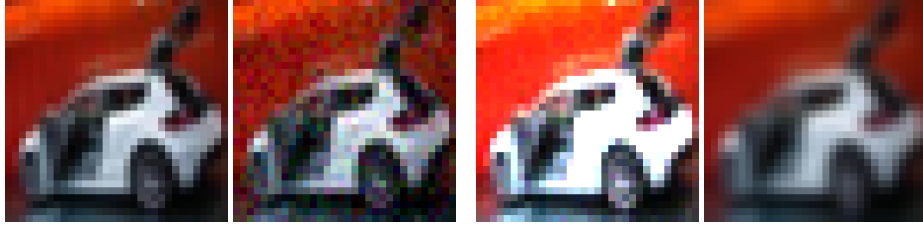


Figure 4: Clean and noisy car images of the CIFAR10 dataset. From left to right, the images are a clean image, an image with the Gaussian distributed noise, an image with Poisson distributed noise, and a Gaussian blurred image.

Table 2: Classification performance on the noisy CIFAR10.

	CIFAR10/ResNet44					
	Gaussian Noise 1	Gaussian Noise 2	Gaussian Noise 3	Gaussian Noise 4	Poisson Noise	Gaussian Blur
ReLU	<b>69.74</b>	<b>68.96</b>	<b>29.95</b>	30.12	73.71	57.16
LReLU	69.04	68.48	29.64	30.29	74.84	57.16
Mish	66.02	65.48	26.33	26.79	75.28	55.74
SiLU	65.93	65.25	26.19	26.61	74.32	55.04
HardSiLU	68.23	67.46	28.83	29.43	72.77	56.56
LA-SiLU	68.45	68.07	28.98	29.53	<b>83.92</b>	<b>59.59</b>
LA-HardSiLU	<b>69.97</b>	<b>69.56</b>	<b>32.27</b>	<b>32.62</b>	<b>81.82</b>	<b>60.23</b>

distributed noise [15], and Gaussian blur [6]. Specifically, we experimented with six different noisy cases: i) Gaussian distributed noise with mean and standard deviation as 0 and 0.05, ii) 0.1 and 0.05, iii) 0 and 0.1, iv) 0.1 and 0.1, v) Poisson distributed noise, and vi) Gaussian blur noise with kernel size and standard deviation as (3, 3) and 1 (See Figure 4 for the examples of noisy data). We added the noise after re-scaling the data between 0 and 1.

Table 2 and 3 shows the classification performance of ResNet44 on noisy CIFAR10 and CIFAR100 datasets as the mean accuracy over 30 runs (see Appendix G for the results of ResNet20 and ResNet32). The best results are underlined and bolded, while the second best are bolded. We do not report the experiments of ResNet44 with PReLU on CIFAR10 as a network exploded during training. On all noisy datasets, networks with LA-HardSiLU showed better performance. In statistical significance test, networks with LA-HardSiLU outperformed those with element-level activation functions (T-test or Wilcoxon signed-rank test with  $p$ -value < 0.05), except networks with ReLU and LReLU on noisy CIFAR10 with Gaussian noise 1 and 2. This result demonstrates that LA-HardSiLU exhibits greater noise-robustness to intense noise compared to other functions.

### 4.2.3 ImageNet

Table 4 shows the classification performance of the LayerAct functions and the element-level activation functions for comparison with clean and noisy ImageNet datasets. We report the accuracy of 10-crop testing on validation dataset. The best results are underlined and bolded, while the second best are bolded. For ImageNet, we experimented on four different noisy cases: i) Gaussian distributed noise with 0 and standard deviation 0.1, ii) Gaussian distributed noise with 0.1 and standard deviation 0.1, iii) Poisson distributed noise, and iv) Gaussian blur noise with kernel size and standard deviation as (7, 7) and 3. The networks with LayerAct functions outperformed those with other activation functions on all datasets. The LayerAct functions, even LA-HardSiLU that showed worse performance on the clean CIFAR10 and CIFAR100 datasets than SiLU or LReLU, outperformed other activation functions. We report more trials with different random seed for weight initialization in Appendix G.

Table 3: Classification performance on the noisy CIFAR100.

	CIFAR100/ResNet44					
	Gaussian Noise 1	Gaussian Noise 2	Gaussian Noise 3	Gaussian Noise 4	Poisson Noise	Gaussian Blur
ReLU	32.01	31.98	10.50	10.37	22.62	32.66
LReLU	32.14	32.31	10.77	10.78	22.97	33.32
PReLU	32.78	32.51	10.75	10.40	21.84	31.52
Mish	30.30	30.36	9.67	9.73	22.82	33.11
SiLU	30.83	30.86	10.33	10.21	20.11	32.91
HardSiLU	33.49	33.59	11.39	11.34	19.44	34.21
LA-SiLU	<b>34.81</b>	<b>35.44</b>	<b>11.85</b>	<b>12.57</b>	<b>34.38</b>	<b>36.84</b>
LA-HardSiLU	<b>40.51</b>	<b>41.25</b>	<b>16.08</b>	<b>17.07</b>	<b>36.19</b>	<b>39.72</b>

Table 4: Classification performance on the clean and noisy ImageNet.

	ImageNet/ResNet50				
	Without noise	Gaussian noise 1	Gaussian noise 2	Poisson noise	Gaussian blur
ReLU	77.71	70.73	69.03	6.55	<b>67.91</b>
LReLU	77.83	70.41	68.69	9.29	67.88
PReLU	74.99	64.77	63.39	8.32	63.64
Mish	77.41	69.22	67.60	14.25	67.45
SiLU	77.85	69.68	68.54	9.52	67.42
HardSiLU	76.30	67.49	65.89	24.64	65.51
LA-SiLU	<b>78.62</b>	<b>71.40</b>	<b>70.76</b>	<b>43.07</b>	<b>69.12</b>
LA-HardSiLU	<b>78.23</b>	<b>71.81</b>	<b>71.23</b>	<b>47.36</b>	<b>67.91</b>

## 5 Discussion

Activation functions form the backbone of neural networks. To the best of our knowledge, this study is the first to develop a layer-level activation mechanism for achieving both zero-like mean activation and noise-robustness, which are the important properties of effective activation. The theoretical and experimental analyses in this study support the potential of the LayerAct functions to develop robust deep learning frameworks with high-performance. Although we suggest only two LayerAct functions in this study, it is possible to devise other LayerAct functions with suitable activation scale functions which can ensure zero-like mean activation and noise-robustness.

In this paper, we only introduced unbounded LayerAct functions, LA-SiLU and LA-HardSiLU. Such activation functions may not be directly utilized with the RNN-based networks. For RNN-based networks, bounded activation functions (i.e., functions that saturate both negative and positive sides) such as Sigmoid or Tanh are commonly utilized [10, 3]. Therefore, the development of bounded LayerAct functions is one of our future research directions.

## 6 Conclusion

In this study, we introduce a novel layer-level activation mechanism and LayerAct functions. Unlike the element-level activation functions, where non-linearity is directly dependent on the input of a single element, LayerAct functions provide non-linearity with layer-direction normalized input of all elements in the layer. This unique activation mechanism enables LayerAct functions to achieve one-sided saturation while also allowing larger negative outputs. Moreover, the activation scale with normalized input enables the LayerAct functions to reduce the mean and variance of activation fluctuation, implying that networks with LayerAct functions have lower variance of noise-robustness across samples. These properties of LayerAct functions are verified through experiments on the MNIST dataset. Networks trained using LA-SiLU, one of the possible LayerAct functions, demonstrated similar or better performance than those for the other activation functions on the clean image datasets. Moreover, LA-HardSiLU outperformed the other activation functions at most of the experiments on noisy datasets.

## References

- [1] BA, J. L., KIROS, J. R., AND HINTON, G. E. Layer normalization. *arXiv:1607.06450* (2016).
- [2] BJORCK, N., GOMES, C. P., SELMAN, B., AND WEINBERGER, K. Q. Understanding batch normalization. In *Proceeding of NeurIPS* (2018), vol. 31.
- [3] CHO, K., MERRIENBOER, B., GULCEHRE, C., BOUGARES, F., SCHWENK, H., AND BENGIO, Y. Learning phrase representations using rnn encoder-decoder for statistical machine translation. In *EMNLP* (2014), p. 1724–1734.
- [4] CLEVERT, D.-A., UNTERTHINER, T., AND HOCHREITER, S. Fast and accurate deep network learning by exponential linear units (elus). In *Proceedings of ICLR* (2016).
- [5] ELFWING, S., UCHIBE, E., AND DOYA, K. Sigmoid-weighted linear units for neural network function approximation in reinforcement learning. *Neural Networks 107* (2018), 3–11. Special issue on deep reinforcement learning.
- [6] FLUSSER, J., FAROKHI, S., HÖSCHL, C., SUK, T., ZITOVÁ, B., AND PEDONE, M. Recognition of images degraded by gaussian blur. *IEEE Transactions on Image Processing 25*, 2 (2016), 790–806.
- [7] HAHNLOSER, R. H., SARPESHKAR, R., MAHOWALD, M. A., DOUGLAS, R. J., AND SEUNG, H. S. Digital selection and analogue amplification coexist in a cortex-inspired silicon circuit. *Nature 405*, 6789 (2000), 947–951.
- [8] HE, K., ZHANG, X., REN, S., AND SUN, J. Delving deep into rectifiers: Surpassing human-level performance on imagenet classification. In *Proceedings of ICCV* (2015).
- [9] HE, K., ZHANG, X., REN, S., AND SUN, J. Deep residual learning for image recognition. In *Proceedings of CVPR* (2016).
- [10] HOCHREITER, S., AND SCHMIDHUBER, J. Long short-term memory. *Neural Computation 9*, 8 (1997), 1735–1780.
- [11] IOFFE, S., AND SZEGEDY, C. Batch normalization: Accelerating deep network training by reducing internal covariate shift. In *Proceedings of ICML* (2015), vol. 37, pp. 448–456.
- [12] KRIZHEVSKY, A. Learning multiple layers of features from tiny images. *Master’s thesis, University of Toronto* (2009).
- [13] KRIZHEVSKY, A., SUTSKEVER, I., AND HINTON, G. E. Imagenet classification with deep convolutional neural networks. *Commun. ACM 60*, 6 (may 2017), 84–90.
- [14] LABATIE, A., MASTERS, D., EATON-ROSEN, Z., AND LUSCHI, C. Proxy-normalizing activations to match batch normalization while removing batch dependence. In *Proceedings of NeurIPS* (2021), vol. 34, pp. 16990–17006.
- [15] LE, T., CHARTRAND, R., AND ASAKI, T. J. A variational approach to reconstructing images corrupted by poisson noise. *Journal of mathematical imaging and vision 27* (2007), 257–263.
- [16] LEE, C.-Y., XIE, S., GALLAGHER, P., ZHANG, Z., AND TU, Z. Deeply-supervised nets. In *Proceedings of AISTATS* (2015), vol. 38, pp. 562–570.
- [17] LUBANA, E. S., DICK, R., AND TANAKA, H. Beyond batchnorm: Towards a unified understanding of normalization in deep learning. In *Proceedings of NeurIPS* (2021), vol. 34, Curran Associates, Inc., pp. 4778–4791.
- [18] MAAS, A. L., HANNUN, A. Y., NG, A. Y., ET AL. Rectifier nonlinearities improve neural network acoustic models. In *Proceedings of ICML* (2013), vol. 30, p. 3.
- [19] MISRA, D. Mish: A self regularized non-monotonic activation function. *arXiv:1908.08681* (2020).
- [20] NAIR, V., AND HINTON, G. E. Rectified linear units improve restricted boltzmann machines. In *Proceedings of ICML* (2010).
- [21] PASZKE, A., GROSS, S., MASSA, F., LERER, A., BRADBURY, J., CHANAN, G., KILLEEN, T., LIN, Z., GIMELSHEIN, N., ANTIGA, L., DESMAISON, A., KOPF, A., YANG, E., DEVITO, Z., RAISON, M., TEJANI, A., CHILAMKURTHY, S., STEINER, B., FANG, L., BAI, J., AND CHINTALA, S. Pytorch: An imperative style, high-performance deep learning library. In *Proceedings of NeurIPS* (2019), vol. 32.

- [22] QIU, S., XU, X., AND CAI, B. Frelu: Flexible rectified linear units for improving convolutional neural networks. In *Proceedings of ICPR (2018)*, pp. 1223–1228.
- [23] RAMACHANDRAN, P., ZOPH, B., AND LE, Q. V. Searching for activation functions. In *Proceedings of ICLR workshop (2018)*.
- [24] RUSSAKOVSKY, O., DENG, J., SU, H., KRAUSE, J., SATHEESH, S., MA, S., HUANG, Z., KARPATY, A., KHOSLA, A., BERNSTEIN, M., ET AL. Imagenet large scale visual recognition challenge. *International journal of computer vision* 115, 3 (2015), 211–252.
- [25] VIJAYKUMAR, V., VANATHI, P., AND KANAGASABAPATHY, P. Fast and efficient algorithm to remove gaussian noise in digital images. *IAENG International Journal of Computer Science* 37, 1 (2010), 300–302.
- [26] XU, B., HUANG, R., AND LI, M. Revise saturated activation functions. *arXiv:1602.05980* (2016).

## A Definition of zero-like mean activation

The activation output of the  $i^{\text{th}}$  unit of  $m^{\text{th}}$  sample ( $m \in \{1, 2, \dots, M\}$ ) is defined as  $a_{i,m} = f(y_{i,m})$ , where  $f$ ,  $y_{i,m}$ , and  $M$  are activation function, the  $i^{\text{th}}$  activation input of the  $m^{\text{th}}$  sample, and the number of samples, respectively. Ideally, a “zero-like activation mean” occurs when the activation mean of a single unit,  $a_i$ , approximates zero across the samples. Mathematically, this can be represented as:

$$\frac{1}{M} \sum_{m=1}^M a_{i,m} \approx 0.$$

However, approximating the activation mean to zero is challenging for the activation functions that saturate the (large) negative outputs such as ELU, SiLU or FReLU. Due to the saturation, previous studies have defined the “zero-like activation mean” property of an activation function as its ability to “push” the activation mean towards zero. In a mathematical term, this can be presents as  $|\mu_{a_i}| \ll c$ , where  $c$  is a small positive constant [4, 22].

## B Difference between LayerAct and activation with LayerNorm

In this section, we compare the activation outputs between LayerAct and activation functions paired with LayerNorm. When LayerNorm is placed right before activation, the output is  $a_i = n_i^{LN} s(n_i^{LN})$ , where  $n_i^{LN}$  is normalized output of LayerNorm. Conversely, the activation output of a LayerAct function is  $a_i = y_i s(n_i)$ , as defined in Equation 6 in the main article.

The critical distinction between activation with LayerNorm and LayerAct lies in the preservation of input mean and variance statistical information in the activation output. With LayerNorm, the activation function takes a layer-normalized input, resulting in activation outputs that exhibit similar statistical information across samples (as shown in the activation output equation for LayerNorm above). However, this homogenization of statistical information across samples, a characteristic of LayerNorm, is a reason why BatchNorm often outperforms LayerNorm in non-sequential models such as CNNs [14, 17].

LayerAct, on the other hand, preduces more distinguishable activation outputs between samples by preserving statistical variation between samples. This is due to the fact that only the activation scale function of LayerAct uses the layer-normalized input, not the LayerAct function itself (as shown in Equation 6 in the main article).

We would like to note that LayerAct is compatible with BatchNorm, and all the networks used in our CIFAR10, CIFAR100 and ImageNet experiments contain BatchNorm. It is worth noting that the dimension of input normalization between BatchNorm and the activation scale of LayerAct differs, which can result in different effects from BatchNorm to LayerAct. Thus, LayerAct can be effectively used with BatchNorm to enhance the performance of neural networks.

## C RNN-based networks with LayerAct

In the networks where activation and LayerNorm have one-to-one correspondence (i.e. LayerNorm is placed right before the activation), the activation input would be the output of LayerNorm:

$$n_i^{LN} = LN(y_i) = g_i \frac{y_i - \mu}{\sqrt{\sigma_y^2 + \alpha}} + b_i,$$

where  $LN$  denotes LayerNorm, and  $n_i^{LN}$ ,  $g_i$  and  $b_i$  are layer-normalized output, the gain and bias parameters of LayerNorm, respectively. Since  $n_i^{LN}$  is already layer-normalized, the activation outputs of element-level activation function,  $n_i^{LN} s(n_i^{LN})$ , and LayerAct function,  $n_i^{LN} s(n_i)$ , become more similar when the gain and bias parameters of LayerNorm are closer to zero and one, respectively.

However, there are RNN-based networks without one-to-one correspondence between activation and normalization. An example of this is the LSTM-based network with LayerNorm that proposed by Ba

et al. [1]:

$$\begin{pmatrix} f_t \\ i_t \\ o_t, \\ g_t \end{pmatrix} = LN(W_h h_{t-1}; \alpha_1, \beta_1) + LN(W_x x_t; \alpha_2, \beta_2)$$

$$c_t = \sigma(f_t) \odot c_{t-1} + \sigma(i_t) \odot \tanh(g_t)$$

$$h_t = \sigma(o_t) \odot \tanh(LN(c_t; \alpha_3, \beta_3))$$

where  $LN$  and  $\sigma$  denotes LayerNorm and Sigmoid as activation function. In this network, the activation input  $f$ ,  $i$ , and  $o$  of  $\sigma$  are the sum of the two layer-normalized outputs and a bias  $b$ . This means that the input of the activation scale function, the sum of two layer-normalized outputs from the LayerNorm layer, will differ between LayerAct and element-level activation, leading to different activation outputs. Despite LayerAct and LayerNorm having the same normalization direction, LayerAct functions can still be utilized with LayerNorm in such networks.

## D Activation output of LayerAct functions

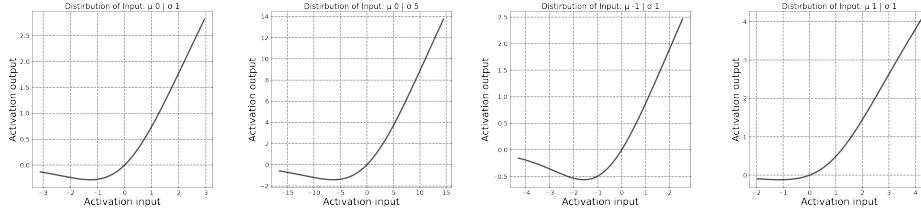


Figure 5: LA-SiLU with different mean and variance value in the input. The distribution of the activation input is: i)  $\mu_y = 0, \sigma_y = 1$ , ii)  $\mu_y = 0, \sigma_y = 5$ , iii)  $\mu_y = -5, \sigma_y = 1$ , and iv)  $\mu_y = 5, \sigma_y = 1$  from the left to right.

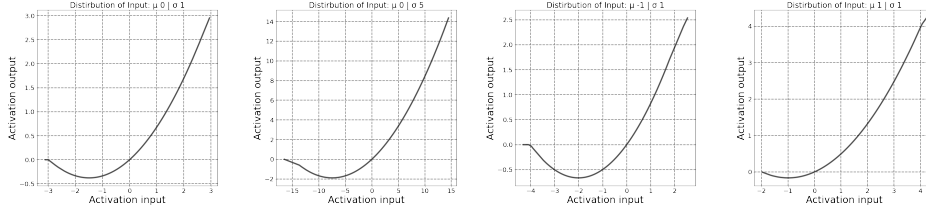


Figure 6: LA-HardSiLU with different mean and variance values in the input. The distribution of the activation input is: i)  $\mu_y = 0, \sigma_y = 1$ , ii)  $\mu_y = 0, \sigma_y = 5$ , iii)  $\mu_y = -5, \sigma_y = 1$ , and iv)  $\mu_y = 5, \sigma_y = 1$  from the left to right.

In this section, we present and discuss an illustration of LayerAct functions. Unlike other activation functions, the mean and variance of the input affect the shape of the activation output in the LayerAct functions (as outlined in Equation 6 in the main article). For better demonstration of this characteristic, we present the outputs of the LayerAct functions for four distinct cases. Each cases uses an input that follows a different normal distribution.

Figures 5 and 6 plot the activation outputs of LA-SiLU and LA-HardSiLU, respectively. These figures demonstrate how the shape of activation output are different depending on the shape, mean and variance in this cases, of the activation input. The figures also show that LayerAct functions can produce negative outputs depending on the mean and variance of the inputs. In some cases, no output exists in the saturation state (see the second figure in Figure 6). It is notable that the LayerAct functions achieved noise-robustness without a large number of elements in the saturation state.

## E Experimental reproduction

We implemented LayerAct functions and networks for experiment with PyTorch [21]. All networks used in our experiments were trained on NVIDIA A100. We used multiple devices to train the networks on ImageNet, and a single device for the other experiments. The versions of Python and the packages were i) Python 3.9.12, ii) numpy 1.19.5 iii) PyTorch 1.11.0, and iv) torchvision 0.12.0. We used cross entropy loss functions for all the experiments. The random seeds of the experiments were  $11 \times i$  where  $i \in \{1, 2, \dots, 30\}$  on CIFAR10 and CIFAR100 and 11 and 22 on ImageNet.

To train networks on MNIST for experimental analysis, we applied batch gradient descent for 80 epochs with the weight decay and momentum fixed to 0.0001 and 0.9, respectively. The learning rate started from 0.01, and was multiplied 0.1 at epochs 40 and 60 as scheduled.

We used ResNet [9] with BatchNorm right before activation for experiments on CIFAR10, CIFAR100 and ImageNet. We initialized the weights following the methods proposed by He et al. [8]. For all experiments, the weight decay, momentum, and initial learning rate were 0.0001, 0.9 and 0.1, respectively.

For CIFAR10 and CIFAR100, we trained ResNet20, ResNet32, and ResNet44 with a basic block using the stochastic gradient descent with a batch size of 128 for about 64000 iterations. We randomly selected 10% of the training dataset as the validation set. The learning rate was scheduled to decrease by the factor of 10 at 32000 and 48000 iterations. For the data augmentation of CIFAR10 and CIFAR100, we followed Lee et al. [16]. We rescaled the data between 0 and 1, padded 4 pixels on each side, and randomly sampled a  $32 \times 32$  crop from the padded image or its horizontal flip. The data was normalized after augmentation. For testing, we did not apply data augmentation, only normalized the data. The hyper-parameter  $\alpha$  of LayerAct functions for the experiments was set to 0.00001.

For the experiment with ImageNet, we trained ResNet50 with the bottleneck block using stochastic gradient descent, and the batch size was 256 for about 600000 iterations. The learning rate was scheduled to decrease by a factor of 10 at 180000, 360000, and 540000 iterations. For the data augmentation on ImageNet, we rescaled the data between 0 and 1, resized it to  $224 \times 224$ , and randomly sampled a  $224 \times 224$  crop from an image or its horizontal flip [13]. We normalized the data after data augmentation. For testing, we resized the data to be  $256 \times 256$  and applied 10-crop. Afterward, the data was normalized. To ensure stable learning, we set the hyper-parameter  $\alpha$  of LayerAct functions to 0.1 which is larger than those for CIFAR10 and CIFAR100.

The noisy datasets were generated by adding noise to the data after it was rescaled between 0 and 1. Following this, the same data augmentation applied to the clean dataset were also used on the noisy dataset.

## F Supplementary material

The supplementary material of this paper and the trained networks are available in our anonymous GitHub repository<sup>1</sup>.

---

<sup>1</sup><https://github.com/LayerAct/LayerAct>

## G Additional figures and tables

In this section, we present additional tables and figures extracted from the experiments.

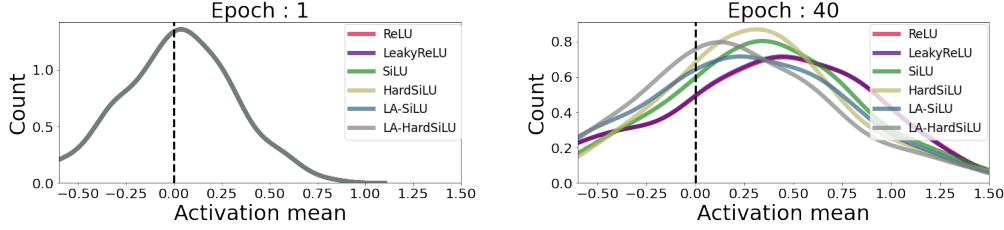


Figure 7: Distribution of the activation **input** means of the elements in a trained network on MNIST at 1<sup>st</sup> and 40<sup>th</sup> epochs.

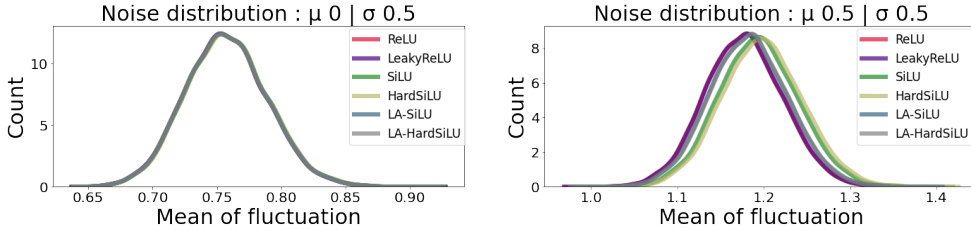


Figure 8: Distribution of activation **input** fluctuation due to noise with different noise distribution.

Figure 7 presents the distribution of the mean activation input. As observed in the mean of activation input at epoch 40 (right), LayerAct functions promote the training of parameter  $W$  such that the output of the linear projection  $y = W^T x$ , which is also activation input, gets closer to zero compared to other functions. This helps the activation output to exhibit a ‘zero-like’ behaviour.

LayerAct functions exhibit a significantly lower mean and variance of activation fluctuation among the samples compared to any other element-level activation function (see Figure 3 in the main article). Figure 8 demonstrates that the distribution of mean fluctuation in activation input appears similar across all functions. This observation confirms that the lower mean and variance of activation output fluctuation of LayerAct functions is not due to a smaller fluctuation in activation input, but is a result of the inherent mechanism of LayerAct.

Table 5: Standard deviation of classification performance on the clean CIFAR10 and CIFAR100.

	CIFAR10			CIFAR100		
	ResNet20	ResNet32	ResNet44	ResNet20	ResNet32	ResNet44
ReLU	0.22	0.39	0.64	<b>0.30</b>	0.53	0.57
LReLU	0.27	0.34	0.45	<b>0.33</b>	<b>0.34</b>	0.70
PReLU	0.24	0.28	-	0.45	0.51	0.72
Mish	0.23	0.25	0.45	<b>0.33</b>	0.49	<b>0.52</b>
SiLU	<b>0.21</b>	<b>0.22</b>	<b>0.25</b>	0.42	0.51	0.53
HardSiLU	0.23	<b>0.22</b>	0.43	0.40	0.54	0.96
LA-SiLU	<b>0.17</b>	<b>0.19</b>	0.28	0.36	<b>0.38</b>	<b>0.44</b>
LA-HardSiLU	<b>0.21</b>	0.31	<b>0.21</b>	0.41	0.46	0.81

Table 5 demonstrate the standard deviation of classification performance on the clean CIFAR10 and CIFAR100 datasets. The lowest results are underlined and bolded, while the second lowest are bolded. The performance of networks with LA-SiLU were similar or more stable compared to other activation functions in most cases.

Table 6: Statistical significance test of LA-SiLU on CIFAR10 dataset.

	CIFAR10					
	ReLU	LReLU	PReLU	Mish	SiLU	HardSiLU
ResNet20	<0.05	<0.05	<0.05	<0.05	<0.05	<0.05
ResNet32	<0.05	<0.05	<0.05	>0.05	>0.05	<0.05
ResNet44	<0.05	<0.05	<0.05	>0.05	<0.05	<0.05

Table 7: Statistical significance test of LA-SiLU on CIFAR100 dataset.

	CIFAR100					
	ReLU	LReLU	PReLU	Mish	SiLU	HardSiLU
ResNet20	<0.05	<0.05	<0.05	<0.05	<0.05	<0.05
ResNet32	<0.05	<0.05	<0.05	<0.05	<0.05	<0.05
ResNet44	>0.05	>0.05	<0.05	>0.05	<0.05	<0.05

Tables 6 and 7 present the results of a statistical significance test between the accuracy of networks with element-level activation functions and those with LA-SiLU on clean CIFAR10 and CIFAR100. When the accuracies of both functions were normally distributed, we performed a T-test. In cases where at least one of them are not, we performed a Wilcoxon signed-rank test otherwise. The notation '>0.05' indicates that the  $p$ -value from either a T-test or a Wilcoxon signed-rank test is larger than the standard significance level of 0.05 (i.e.  $p$ -value > 0.05). This suggests that LA-SiLU is not significantly better or worse than the alternative function. Conversely, '<0.05' denotes that the  $p$ -value is smaller than 0.05, indicating that LA-SiLU is significantly superior to the alternative function (i.e.  $p$ -value < 0.05).

Tables 8, 9, 10, and 11 demonstrate the classification performance of ResNet20 and ResNet32 with activation functions on noisy CIFAR10 and CIFAR100 datasets. Six different noisy cases are presented in the tables: i) Gaussian distributed noise with mean and standard deviation as 0 and 0.05, ii) 0.1 and 0.05, iii) 0 and 0.1, iv) 0.1 and 0.1, v) Poisson distributed noise, and vi) Gaussian blur noise with kernel size and standard deviation as (3, 3) and 1. The performance of networks with LayerAct functions were better than other activation functions in most cases.

Figures 9 and 10 display the average accuracy over 30 runs for ResNet20, ResNet32, and ResNet44 on Gaussian noisy CIFAR10 and CIFAR100 with a fixed mean as 0 and different variance. There was no noticeable difference in network performance across different activation functions when the variance of noise was large (Figures 9 and 10). Meanwhile, LayerAct functions were highly performing when noise have large mean. Figures 11 and 12 present the average accuracy over 30 runs for ResNet20, ResNet32, and ResNet44 on Gaussian noisy CIFAR10 and CIFAR100 with different mean and a fixed variance as  $0.01^2$ , respectively. The robustness of networks with LayerAct functions to the large noise mean is remarkable when compared to those with element-level activation function, especially on CIFAR100 dataset which is more complex than CIFAR10.

In the paper, we reported the classification performance of ResNet50 on ImageNet with random seed 11 for weight initialization. Table 12 demonstrate the experimental result of ResNet50 with activation functions with random seed 22. Network with PReLU exploded during training.

Table 8: Classification performance of ResNet20 on the noisy CIFAR10.

	CIFAR10/ResNet20					
	Gaussian Noise 1	Gaussian Noise 2	Gaussian Noise 3	Gaussian Noise 4	Poisson Noise	Gaussian Blur
ReLU	61.50	60.98	22.33	23.00	75.14	51.10
LReLU	60.72	60.07	22.63	23.25	72.72	51.61
PReLU	60.18	59.35	23.50	23.79	72.48	49.71
Mish	60.17	59.32	22.90	23.31	69.85	51.75
SiLU	61.15	60.27	23.96	24.47	68.64	51.89
HardSiLU	60.17	59.35	22.56	23.16	68.08	52.52
LA-SiLU	<b>63.37</b>	<b>63.14</b>	<b>25.77</b>	<b>26.34</b>	<b>79.91</b>	<b>58.31</b>
LA-HardSiLU	<b>63.29</b>	<b>63.07</b>	<b>26.45</b>	<b>26.79</b>	<b>80.19</b>	<b>58.45</b>

Table 9: Classification performance of ResNet32 on the noisy CIFAR10.

	CIFAR10/ResNet32					
	Gaussian Noise 1	Gaussian Noise 2	Gaussian Noise 3	Gaussian Noise 4	Poisson Noise	Gaussian Blur
ReLU	65.72	65.13	25.37	26.00	74.80	53.44
LReLU	65.57	64.83	25.07	25.65	74.69	54.75
PReLU	65.43	64.66	25.38	25.53	72.56	54.00
Mish	65.30	64.52	26.20	26.49	74.39	53.76
SiLU	64.76	64.06	25.37	25.71	72.26	52.87
HardSiLU	64.62	64.17	24.92	25.74	71.78	53.37
LA-SiLU	<b>66.12</b>	<b>66.09</b>	<b>27.41</b>	<b>28.25</b>	<b>83.56</b>	<b>57.91</b>
LA-HardSiLU	<b>67.44</b>	<b>67.21</b>	<b>30.04</b>	<b>30.67</b>	<b>82.54</b>	<b>58.52</b>

Table 10: Classification performance of ResNet20 on the noisy CIFAR100.

	CIFAR100/ResNet20					
	Gaussian Noise 1	Gaussian Noise 2	Gaussian Noise 3	Gaussian Noise 4	Poisson Noise	Gaussian Blur
ReLU	26.61	26.83	8.57	8.42	23.71	31.50
LReLU	26.95	27.36	<b>8.63</b>	<b>8.80</b>	23.21	31.82
PReLU	24.81	24.59	7.72	7.50	21.26	29.09
Mish	24.94	24.84	7.68	7.51	21.12	30.57
SiLU	26.21	26.17	8.29	8.19	19.78	30.57
HardSiLU	26.19	26.45	8.11	8.12	19.79	30.63
LA-SiLU	<b>27.37</b>	<b>27.62</b>	8.23	8.49	<b>30.80</b>	<b>33.61</b>
LA-HardSiLU	<b>28.62</b>	<b>28.93</b>	<b>8.90</b>	<b>9.12</b>	<b>27.35</b>	<b>34.31</b>

Table 11: Classification performance of ResNet32 on the noisy CIFAR100.

	CIFAR100/ResNet32					
	Gaussian Noise 1	Gaussian Noise 2	Gaussian Noise 3	Gaussian Noise 4	Poisson Noise	Gaussian Blur
ReLU	29.94	29.97	9.85	9.83	22.58	32.20
LReLU	29.51	29.52	9.35	9.24	22.97	32.50
PReLU	29.57	29.25	9.19	8.88	20.76	30.35
Mish	28.29	28.35	8.92	8.75	23.29	31.88
SiLU	29.25	29.29	9.42	9.36	19.93	31.38
HardSiLU	29.90	29.97	9.52	9.47	19.06	31.47
LA-SiLU	<b>31.19</b>	<b>31.86</b>	<b>10.21</b>	<b>10.80</b>	<b>33.62</b>	<b>35.81</b>
LA-HardSiLU	<b>33.18</b>	<b>33.67</b>	<b>11.82</b>	<b>12.49</b>	<b>26.42</b>	<b>36.52</b>

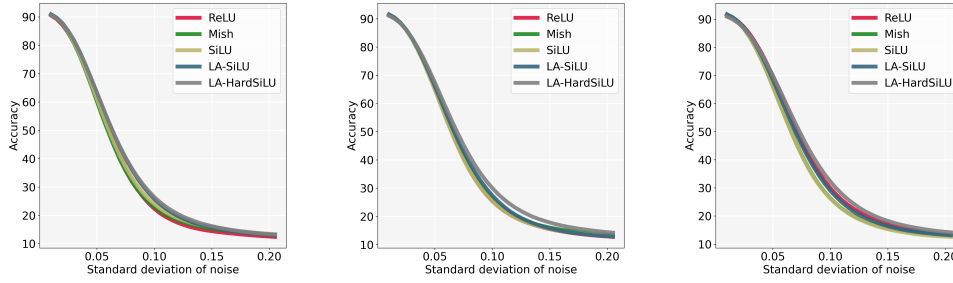


Figure 9: Accuracy plot of ResNet20 (left), ResNet32 (middle), and ResNet44 (right) with activation functions on Gaussian noisy CIFAR10 datasets with fixed mean and different variance.

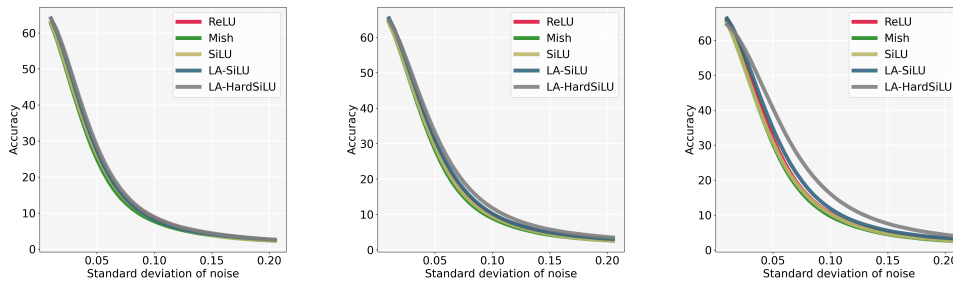


Figure 10: Accuracy plot of ResNet20 (left), ResNet32 (middle), and ResNet44 (right) with activation functions on Gaussian noisy CIFAR100 datasets with fixed mean and different variance.

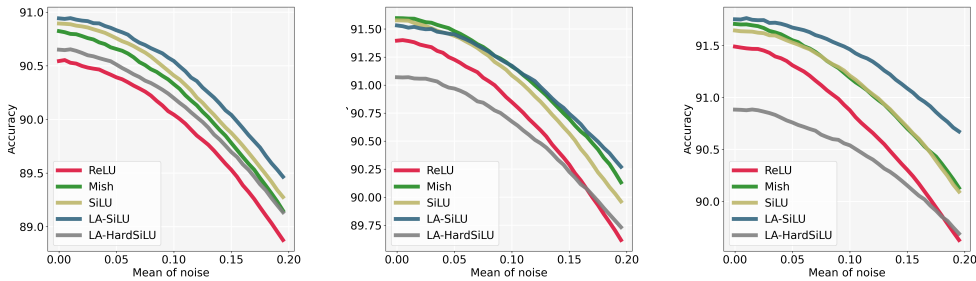


Figure 11: Accuracy plot of ResNet20 (left), ResNet32 (middle), and ResNet44 (right) with activation functions on Gaussian noisy CIFAR10 datasets with different mean and fixed variance.

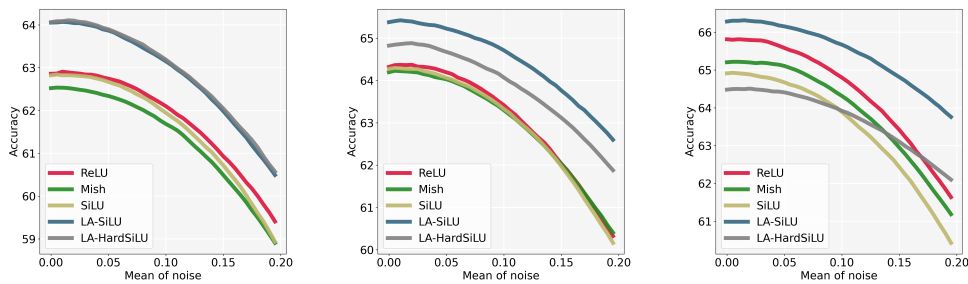


Figure 12: Accuracy plot of ResNet20 (left), ResNet32 (middle), and ResNet44 (right) with activation functions on Gaussian noisy CIFAR100 datasets with different mean and fixed variance.

Table 12: Classification performance on the clean and noisy ImageNet.

	ImageNet/ResNet50				
	Without noise	Gaussian noise 1	Gaussian noise 2	Poisson noise	Gaussian blur
ReLU	78.04	70.15	68.86	8.15	<b>68.79</b>
LReLU	76.86	69.28	68.31	11.26	67.38
Mish	77.66	69.36	67.63	21.34	67.22
SiLU	77.62	69.12	67.67	7.15	<b>67.62</b>
HardSiLU	76.32	67.53	66.00	13.97	64.82
LA-SiLU	<b>78.51</b>	<b>71.85</b>	<b>71.10</b>	<b>49.33</b>	67.08
LA-HardSiLU	<b>78.11</b>	<b>71.67</b>	<b>71.14</b>	<b>38.64</b>	67.37